bioRxiv preprint doi: https://doi.org/10.1101/2020.09.04.282426; this version posted September 4, 2020. The copyright holder for this preprint (which was not certified by peer review) is the author/funder, who has granted bioRxiv a license to display the preprint in perpetuity. It is made available under aCC-BY-NC-ND 4.0 International license.

TITLE PAGE

Title: Non-permissive human conventional CD1c$^+$ dendritic cells enable *trans*-infection of human primary renal tubular epithelial cells and protect BK polyomavirus from neutralization

Mathieu Sikorski[1], Flora Coulon[1], Cécile Peltier[1], Cécile Braudeau[1,2], Alexandra Garcia[1], Matthieu Giraud[1], Karine Renaudin[1,3], Christine Kandel-Aznar[3], Steven Nedellec[4], Philipe Hulin[4], Julien Branchereau[1,5,6], Joëlle Véziers[7,8], Pauline Gaboriaud[9], Antoine Touzé[9], Julien Burlaud-Gaillard[10], Régis Josien[1,2], Dorian McIlroy[1], Céline Bressollette-Bodin[1,11], Franck Halary[1*]

[1] Nantes Université, Inserm, CHU Nantes, Center for Research in Transplantation and Immunology UMR1064, ITUN, Nantes, France

[2] CHU Nantes, Laboratoire d'Immunologie, CIMNA, Nantes, France

[3] CHU Nantes, Service d'Anatomie et Cytologie Pathologiques, Nantes, France

[4] MicroPicell imaging facility, Structure Fédérative de Recherche Santé François Bonamy - FED 4203/UMS Inserm 016/CNRS 3556, Nantes, France

[5] CHU Nantes, Service d'urologie, France

[6] CHU Nantes, Service de transplantations rénales, France

[7] Plate-forme SC3M, Structure Fédérative de Recherche Santé François Bonamy - FED 4203/UMS Inserm 016/CNRS 3556, Nantes, France

[8] INSERM, UMRS 1229, RMeS, UFR Odontologie, CHU Nantes, Nantes, France

[9] Infectiologie et Santé Publique, UMR INRAE 1282, UFR de Sciences Pharmaceutiques, Université de Tours, France

[10] Département des Microscopies, Plateforme IBiSA de Microscopie Electronique, Université de Tours, France

[11] CHU Nantes, Laboratoire de virologie, Nantes, France

*Corresponding author

Email: franck.halary@univ-nantes.fr

Running title: Non permissive human CD1c+ DC enable BKPyV transmission

Abstract word count: 182

Text word count (including Methods, excluding Abstract and Figure legends): 4514

bioRxiv preprint doi: https://doi.org/10.1101/2020.09.04.282426; this version posted September 4, 2020. The copyright holder for this preprint (which was not certified by peer review) is the author/funder, who has granted bioRxiv a license to display the preprint in perpetuity. It is made available under aCC-BY-NC-ND 4.0 International license.

Abstract

The BK polyomavirus (BKPyV) is a ubiquitous human virus that persists in the renourinary epithelium. Immunosuppression can lead to BKPyV reactivation in the first year post-transplantation in kidney (KTR) and hematopoietic stem cell transplant recipients. In KTR, persistent DNAemia has been correlated to the occurrence of polyomavirus-associated nephropathy (PVAN) that can lead to graft loss if not properly controlled. Based on recent observations that conventional dendritic cells (cDC) specifically infiltrate PVAN lesions, we hypothesized that those cells could play a role in BKPyV infection. We first demonstrated that monocyte-derived DC (MDDC), an *in vitro* model for mDC, captured BKPyV particles through an unconventional GRAF-1 endocytic pathway. Neither BKPyV particles nor BKPyV-infected cells were shown to activate MDDC. Endocytosed virions were efficiently transmitted to permissive cells and shown to be protected from the antibody-mediated neutralization. Finally, we demonstrated that freshly isolated CD1c+ mDC from the blood and kidney parenchyma behaved similarly to MDDC thus extending our results to cells of clinical relevance. This study sheds light on a potential unprecedented CD1c+ mDC involvement in the BKPyV infection as a promoter of viral spreading.

Introduction

The BK polyomavirus (BKPyV) is a small non-enveloped DNA virus. Its icosahedral capsid is mainly composed of the major capsid protein VP1(1-3). Its prevalence in the worldwide population ranges from 80 to 90%(4, 5). Asymptomatic primary infection mostly occurs during childhood(6, 7) followed by a persistent infection in the renourinary epithelium(8). Evidence of BKPyV reactivation was mainly reported in kidney and hematopoietic stem cell allografts(9-12) first marked by viral shedding in urine possibly progressing to BKPyV-DNAemia.

bioRxiv preprint doi: https://doi.org/10.1101/2020.09.04.282426; this version posted September 4, 2020. The copyright holder for this preprint (which was not certified by peer review) is the author/funder, who has granted bioRxiv a license to display the preprint in perpetuity. It is made available under aCC-BY-NC-ND 4.0 International license.

Persistent BKPyV-DNAemia above 10^4 DNA copies/ml has been correlated to PVAN (overall 1-5% of KTR)(13-15). To date, BKPyV remains a significant cause of kidney failure(11, 16).

Over the last ten years, anti-BKPyV cellular and humoral immune responses have been investigated demonstrating a prominent role of both specific CD4+ and CD8+ cytotoxic T lymphocytes (CTL), mainly recognizing the large T antigen (LTAg)- and VP1-derived peptides associated with various HLA molecules(17-20). Although anti-BKPyV responses are likely to be protective enough in healthy individuals, only ten percent of those shed virions in urine suggesting a limited impact of escape mechanisms(5). DC are known to orchestrate anti-viral immune responses mainly through their ability to cross-present viral antigens, thus efficiently priming or activating naïve or memory specific T cells respectively(21). To date, anti-polyomavirus (PyV) CTL responses in mice and humans were analyzed on autologous PBMC or DC stimulation using viral peptide pools thus bypassing the requirement for antigen processing, including endocytosis, and presentation by HLA class I molecules(18, 21, 22). Only few studies addressed the ability of PyV to bind to, promote maturation or infect DC. In mice, Drake and colleagues showed that splenic DC are activated following infection by a murine PyV (MuPyV) strain thus allowing them to prime a CTL response(22). Using another experimental setup, Lenz et al demonstrated that although HPV16, a carcinogenic papillomavirus, and bovine PyV virus-like particles (VLP) enabled bone marrow-derived DC maturation, BKPyV or JCPyV VLP did not(23). More recently, hamster PyV (HaPyV)- and Trichodysplasia Spinulosa-associated PyV-derived VLP were shown to moderately activate murine splenocytes(24). Similarly, SV40 was shown to infect and activate MDDC from rhesus macaques(25). Human MDDC were shown to support β-propiolactone-inactivated BKPyV-derived antigen presentation while remaining unresponsive to native BK- and JCPyV particles(26) possibly due to distinct viral antigen processing induced by inactivation(27). Gedvilaite and colleagues also reported that human MDDC were responsive to MuPyV and

bioRxiv preprint doi: https://doi.org/10.1101/2020.09.04.282426; this version posted September 4, 2020. The copyright holder for this preprint (which was not certified by peer review) is the author/funder, who has granted bioRxiv a license to display the preprint in perpetuity. It is made available under aCC-BY-NC-ND 4.0 International license.

HaPyV VLP(26). Mostly, DC, although limited to *in vitro* generated cells, seemed to be unresponsive to BK- or JC PyV direct exposure and poorly responsive to BKPyV-derived antigens in KTR and immunocompetent individuals, as recently proposed by Kaur et al(28). The mechanisms behind such DC unresponsiveness remain to be explored regardless of the presence of immunosuppressive drugs.

In the healthy kidney, cDC, including the CD1c+ DC subset, are located within the interstitium(29), close to the renal proximal tubular epithelial cells (hRPTEC), a host cell for BKPyV(30). HRPTEC were shown to negatively regulate cDC activation subsequently leading to the retention of cDC in renal tissues as immature cells(31-33) putatively decreasing antigen presentation by DC. Early stage PVAN is marked by a $CD1c^+$ cDC infiltrate(34) and mild inflammation(30, 35, 36). Whether cDC play a role in the pathophysiology of the BKPyV infection apart from their ability to trigger and sustain specific immune responses is still unclear.

Here, we demonstrate for the first time that myeloid DC, ie MDDC and freshly isolated $CD1c^+$ cDC from the blood and the kidney of healthy donors, but not plasmacytoid DC were capable of capturing BKPyV particles through the CLIC/GEEC endocytic pathway and transmitting them to hRPTEC without getting activated or infected. We also showed that endocytosed BKPyV particles were protected from antibody-mediated neutralization offering to cDC subsets the possibility to participate in BKPyV spreading in the kidney at least in early steps of the reactivation.

Methods

Ethic statements

bioRxiv preprint doi: https://doi.org/10.1101/2020.09.04.282426; this version posted September 4, 2020. The copyright holder for this preprint (which was not certified by peer review) is the author/funder, who has granted bioRxiv a license to display the preprint in perpetuity. It is made available under aCC-BY-NC-ND 4.0 International license.

Biopsies from healthy parts of primitive renal carcinoma patients and blood samples from KTR were collected according to institutional guidelines (CPP Ouest authorization, 11/08/2011) and under patients' informed consent. All samples are conserved in the ITUN bio collection declared at the french Ministère de l'Enseignement Supérieur et de la Recherche under the reference DC-2011-1399 (09/05/2011).

Cell isolation and culture

Elutriated blood monocytes were obtained from healthy volunteers (DTC cell-sorting facility, CHU Nantes, France) and differentiated into monocyte derived-dendritic cells (MDDC) as described by Sallusto et al(37). Human myeloid CD1c+ DC were isolated from blood and kidney by positive immuno-magnetic selection using anti-CD1c/BDCA-1 microbeads according to the manufacturer's instructions (Miltenyi Biotec, Bergisch Gladbach, Germany) or on a FACS ARIA (BD Biosciences, Franklin Lakes, NJ), respectively. CD1c+ DC were recovered from renal cell suspensions of enzymatically digested macroscopically healthy parts of tumor-bearing kidneys (10-15g). Cell purity typically yielded more than 95%. HRPTEC (Sciencell Research Laboratories, Carlsbad, CA) were cultured in complete EpiCM medium (Sciencell Research Laboratories). LNCaP cells (Caliper LifeSciences, Hopkinton, MA) and HEK 293 TT cells (NCI, Frederick, MD) were cultured in RPMI 1640 or DMEM media respectively, both complemented with 2mM L-glutamine and 10% FBS.

Virus and virus-like particle preparation

The BKPyV Dunlop strain was a kind gift by Dr Christine H Rinaldo (UiT, Norway). The gIa, gIb2 and gIVb1 VP1 expression vectors were kindly provided by Dr Christopher Buck (NCI,

bioRxiv preprint doi: https://doi.org/10.1101/2020.09.04.282426; this version posted September 4, 2020. The copyright holder for this preprint (which was not certified by peer review) is the author/funder, who has granted bioRxiv a license to display the preprint in perpetuity. It is made available under aCC-BY-NC-ND 4.0 International license.

128 USA)(38). Preparation and titration of the Dunlop strain were performed as described
129 elsewhere(39). Virus-like particles (VLP) were purified on an iodixanol gradient(40). VLP
130 physical titers were determined on a qNano device using NP100 nanopores (detection range
131 from 50 to 330 nm) and CPC70 calibration particles (Izon Science Ltd, Oxford, UK). Both viral
132 particles and VLP were labelled with Alexa Fluor®647 protein labelling kit according to
133 manufacturer's instructions (Molecular Probes, Eugene, OR). Modified-vaccinia Ankara virus
134 (MVA) was kindly provided by Pr Don Diamon (CoH, Los Angeles, CA).

135

136 **_Cis_ and _Trans_-infection assays**

137 _Cis_- and _trans_-infection experiments were performed as described previously(41, 42). DC and
138 hRPTEC were infected with BKPyV at MOI 0.1 (Dunlop strain). For trans-infection, BKPyV-
139 loaded DC were washed in PBS after two hours at 37°C then put in contact with a subconfluent
140 hRPTEC monolayer. Controls were prepared similarly. After three to seven days post-infection
141 (dpi), LTAg staining was performed to evaluate infection rates as described before (Moriyama
142 and Sorokin, 2009) and imaged on an Axiovert A1 epifluorescence microscope (Carl Zeiss
143 Microscopy GmbH, Germany) or on a Cellomics ArrayScan VTI HCS Reader (Thermo
144 Scientific) for quantification. 25-50 fields, containing 5000-10000 cells were acquired for each
145 well using HCS Studio Cellomics Scan Version 6.5.0 software at various time points pi. VP1
146 expression was assessed by western blot (ab53977; Abcam) against β-actin (clone C4; Santa
147 Cruz Biotechnology Inc., Dallas, Texas).

148

149 **Quantitative RT-PCR analyses**

bioRxiv preprint doi: https://doi.org/10.1101/2020.09.04.282426; this version posted September 4, 2020. The copyright holder for this preprint (which was not certified by peer review) is the author/funder, who has granted bioRxiv a license to display the preprint in perpetuity. It is made available under aCC-BY-NC-ND 4.0 International license.

Total RNA was isolated using the TRIzol reagent (Invitrogen) according to the manufacturers' instructions. Reverse transcription was performed using M-MLV Reverse Transcriptase and random primers following manufacturer's instructions (Invitrogen, USA). Quantitative PCR on reverse transcribed mRNA was performed using Mastermix (Applied Biosystems) or Premix ExTaq 2x (Takara) reagents and the StepOne Plus (Applied Biosystems) or Rotor-Gene (Qiagen) devices. Primers and probe used to detect *LTAg* mRNA were the following: AgT1 5'-ACTCCCACTCTTCTGTTCCATAGG-3', AgT2 5'-TCATCAGCCTGATTTTGGAACCT-3' and AGTS 5'-FAM-TTGGCACCTCTGAGCTAC-BHQ1-3'. Expression levels were normalized to GAPDH using the 2-ΔΔ cycle threshold method.

Gene expression profiling and datasets deposition

BKPyV-mediated cell reprogramming was analysed after 24 hours by 3′digital gene expression (DGE) RNAseq according to Kilens et al.(43). DGE profiles were generated by counting for each sample the number of unique UMIs associated with each RefSeq genes. DESeq 2 was used to normalize expression with the DESeq function. The analysis design used to perform differential expression with DESeq2 between the infected *vs* non-infected conditions took into account the individual DC donors as a confounding variable. Data supporting our results are openly available in the GEO repository under the following ID: GSE154810.

Flow cytometry analyses

Titrated Alexa Fluor®647 labelled-VLP were used to stain cDC, LNCaP and HEK 293 TT cells at the indicated concentration. VLP attachment was detected by flow cytometry gated on DAPI negative cells. To assess DC activation, cells were incubated for 24 hours with 10^3 VLP/cell,

bioRxiv preprint doi: https://doi.org/10.1101/2020.09.04.282426; this version posted September 4, 2020. The copyright holder for this preprint (which was not certified by peer review) is the author/funder, who has granted bioRxiv a license to display the preprint in perpetuity. It is made available under aCC-BY-NC-ND 4.0 International license.

10^3 BKPyV particles/cell or with 100ng/mL LPS and 1µg/mL R848 (Invivogen, San Diego, CA). Antibodies to CD40 (clone 5C3; BD Biosciences), CD80 (clone L307, BD Biosciences), CD83 (clone HB15e, BD Biosciences), CD86 (clone IT2.2, BD Biosciences), CCR6 (clone 11A9, BD Biosciences), CCR7 (clone 3D12, BD Biosciences) and HLA-DR (clone G46-6, BD Biosciences) were used to monitor DC maturation. Whole blood staining was performed on 500µl blood samples from healthy donors with or without Fc fragment receptor blockers (Miltenyi Biotec). Whole blood staining was done with Alexa Fluor®647 labelled-VLP (2.5µg/ml) and cell subsets were discriminated using the following antibody panel : CD45 (Clone J33; Beckman Coulter, Brea, CA), CD11c (Clone BU15; Beckman Coulter), HLA-DR (Clone L243; BD Biosciences), CD123 (Clone 9F5; BD Biosciences) and Lineage (Lin 1; BD Biosciences). FACS analyses were mainly performed on a LSR II flow cytometer (BD Biosciences).

Fluorescence microscopy

MDDC were distinguished from hRPTEC by DC-SIGN staining (clone DCN46; BD Biosciences) when required. High-resolution confocal microscopy by structured illumination was performed to assess BKPyV entry into MDDC. Cells were incubated with determined VLP concentrations for one hour at 37°C in culture medium, washed and fixed with 3.7% PFA (PFA; Electron Microscopy Sciences, Hatfield, PA). Plasma membrane (PM) was stained with 5µg/mL Alexa Fluor®488-conjugated WGA (Thermo Fisher Scientific). Images were acquired on a Nikon N-SIM microscope with a dedicated oil immersion objective (x100, NA 1.49 Plan Apo). Three dimensional optical sectioning was done respecting Nyquist sampling rate (15 structure illuminations per plane, per channel), and super resolution image reconstruction was performed using Nikon Imaging Software algorithms. BKPyV particle colocalization with

bioRxiv preprint doi: https://doi.org/10.1101/2020.09.04.282426; this version posted September 4, 2020. The copyright holder for this preprint (which was not certified by peer review) is the author/funder, who has granted bioRxiv a license to display the preprint in perpetuity. It is made available under aCC-BY-NC-ND 4.0 International license.

CTxB, GRAF-1 and EEA-1 markers was performed as described above with or w/o 2µg/mL Alexa Fluor®555 conjugated CTxB (Thermo Fisher Scientific), and with anti-GRAF1 (4µg/mL; Novus Biological, Littleton, CO) or anti-EEA1 antibody (BD Biosciences) antibodies in 0.1% BSA PBS O/N at 4°C. Nuclei were counterstained with DAPI. Cells were mounted in ProLong™ mounting medium (Thermo Fisher Scientific) and observed on a LSM Nikon A1RSi microscope (Nikon, Tokyo, Japan) at x60 (NA 1.4). 3D reconstruction was done using the Imaris software (Bitplane, Zurich, Switzerland).

Transmission electron microscopy

MDDC were prepared for transmission electron microscopy as described elsewhere(42). Ultrathin sections were observed on a JEM 1010 microscope (Jeol Europe SAS, Croissy Sur Seine, France). TEM images of BKPyV particle preparations in negative contrast were obtained as described previously(44, 45).

ELISA

Supernatants from various MDDC cultures were harvested at indicated times and frozen at -80°C until being analyzed. IL-10 and IL-12p70 were quantified in those culture supernatants by ELISA with BD OptEIA™ human IL-10 and IL-12p70 sets following the manufacturer's instructions (BD Bioscience).

Statistics

bioRxiv preprint doi: https://doi.org/10.1101/2020.09.04.282426; this version posted September 4, 2020. The copyright holder for this preprint (which was not certified by peer review) is the author/funder, who has granted bioRxiv a license to display the preprint in perpetuity. It is made available under aCC-BY-NC-ND 4.0 International license.

Statistical analyses were performed with the PRISM software (GraphPad Software Inc., version 5.04, La Jolla, CA). Almost exclusively one-way ANOVA with multiple comparison tests were performed to assess significance in this study. Exceptionally, correlation and linear regression studies, Mann-Whitney or Friedman tests were also applied to some data sets. *P*-values lower than 0.05 were considered significant.

Results

Human monocyte-derived dendritic cells bind BKPyV particles in a dose- and sialic acid-dependent manner

First, we assessed whether MDDC could bind BKPyV particles using fluorescent-labelled genotype Ib2 (gIb2) BKPyV VLP. VLP integrity was checked by negative contrast TEM (Figure 1A). GIb2 VLP binding was then tested with two BKPyV permissive cell types, namely hRPTEC and HEK293TT but also to MDDC and LNCaP, a BKPyV non-permissive prostatic cancer cell line(46) at various VLP/cell ratios. MDDC effectively bound gIb2 VLP in a dose-dependent manner but to a lesser extent compared to hRPTEC or HEK293TT (Figure 1B), and as expected BKPyV particles were unable to attach to LNCaP cells. MDDC were also shown to bind gIa infectious particles (Dunlop strain; (47)) and VLP at comparable levels (Figure 1C). We further demonstrated that genotypes Ia, Ib2 and IVb1 VLP had similar binding properties to MDDC (Figure 1D). Sialic acids decorating *b*-series gangliosides are known as crucial components for BKPyV infection of hRPTEC and HEK293TT(46). Then, we demonstrated that when MDDC are treated with an appropriate neuraminidase, an enzyme known to specifically remove sialic acid moieties from the PM, gIa, gIb2 and gIVb1 VLP binding was strongly impaired (Figure 1E). Altogether, these results clearly established that MDDC could bind

bioRxiv preprint doi: https://doi.org/10.1101/2020.09.04.282426; this version posted September 4, 2020. The copyright holder for this preprint (which was not certified by peer review) is the author/funder, who has granted bioRxiv a license to display the preprint in perpetuity. It is made available under aCC-BY-NC-ND 4.0 International license.

241 BKPyV from the most frequent genotypes in Europe and Asia in a dose and sialic acid-
242 dependent manner.

243

244 **BKPyV particles are endocytosed in pleiomorphous tubular and macropinosome-like**
245 **endosomes in MDDC**

246 Immature MDDC exhibit high endocytic properties for soluble and particulate antigens (37).
247 Therefore, we hypothesized that BKPyV could be endocytosed following attachment to sialic
248 acid residues on PM. High-resolution confocal imaging showed that fluorescent spots
249 representing VLP or virions were found in cytoplasmic structures (Figures 2A and 2B),
250 confirming that MDDC endocytosed BKPyV following surface attachment. VLP were either
251 located in round-shaped or pleiomorphous tubular structures (Figures 2A and 2C). This was
252 confirmed by 3D cell reconstruction (Figure 2D). Then, we performed TEM imaging and
253 confirmed that VLP and virions were mostly internalized after 30 minutes. Indeed VLP were
254 mainly endocytosed into tubular vesicles (40-60nm width) and to a much lower extent in large
255 round-shaped uncoated endosomes (up to approximately 1µm in diameter) by MDDC (Figures
256 3A, 3B, 3C, 3D3E and 3G). Moreover, these BKPyV-containing tubular vesicles were shown
257 to originate from PM invaginations (Figures 3D and 3E). Some of these vesicles closely
258 resembled sorting endosomes (Figure 3C). Higher magnifications micrographs confirmed that
259 BKPyV virions behaved similarly to VLP (Figure 3F) did not reveal PM curvature upon viral
260 attachment as previously reported for SV40 (Figure 3G; (48)). We concluded that BKPyV was
261 mainly endocytosed into tubular vesicles evoking an uncommon endocytic pathway for viral
262 particles in MDDC.

263

264 **BKPyV colocalizes with GRAF-1+ and cholera toxin B+ compartments in MDDC**

bioRxiv preprint doi: https://doi.org/10.1101/2020.09.04.282426; this version posted September 4, 2020. The copyright holder for this preprint (which was not certified by peer review) is the author/funder, who has granted bioRxiv a license to display the preprint in perpetuity. It is made available under aCC-BY-NC-ND 4.0 International license.

To characterize BKPyV containing vesicles in MDDC we used high-resolution confocal microscopy to identify markers co-localizing with BKPyV in MDDC. Early Endosome Antigen-1 (EEA-1), a marker of early endosomes and macropinosomes, was associated with BKPyV in structures with size ranging from 100nm, the detection limit with this technique, to roughly 1µm in diameter (Figures 4A and 4B). The clathrin-independent carriers (CLIC) or GPI-anchored protein-enriched compartments (GEEC) endocytic pathway(49, 50) known to form tubular vesicles has been recently associated with the protein GTPase Regulator Associated with Focal Adhesion Kinase-1 (GRAF1) (51). BKPyV colocalized with GRAF-1 at the PM and in the cytosol (Figure 4C). Cholera toxin B subunit (CTxB) uses GRAF-1 vesicles to enter cells (51) and we observed a partial VLP/CTxB colocalization in MDDC (Figure 4D). Altogether, our results showed for the first time in MDDC a major BKPyV endocytosis into GRAF-1+ and CTxB+ compartments, two hallmarks of the CLIC/GEEC pathway.

MDDC can transfer virions to renal epithelial cells but are refractory to BKPyV infection

Next, we wondered whether BKPyV-pulsed MDDC, hereafter termed "BKPyV-infected MDDC", could transfer the virus to a permissive cellular third party in *trans*. Here, we took advantage of a *trans*-infection assay previously set up in our laboratory(41, 52). It assesses the ability of a cell type to capture and transfer virions to permissive cells in its vicinity after removing excess unbound/non-internalized virions. LTAg expression was analyzed in these conditions at defined time points (Figure 5A). Infection of hRPTEC, termed *cis*-infection, was estimated between 10 to 18% in all experiments at seven days pi (Figure 5A). No LTAg was detected in BKPyV-infected MDDC suggesting that BKPyV infection is not initiated in MDDC (Figure 5A). To confirm these results with a more sensitive technique, we analyzed *LTAg* expression by RT-qPCR in a similar experimental design. Quantitative results are shown in

bioRxiv preprint doi: https://doi.org/10.1101/2020.09.04.282426; this version posted September 4, 2020. The copyright holder for this preprint (which was not certified by peer review) is the author/funder, who has granted bioRxiv a license to display the preprint in perpetuity. It is made available under aCC-BY-NC-ND 4.0 International license.

Figure 5B. As expected, no LTAg mRNA was detected in BKPyV-infected MDDC whereas the *cis*-infection of hRPTEC or the *trans*-infection conditions displayed high amounts of *LTAg* mRNA. These results were confirmed by assessing the expression of the major capsid protein VP1, a late infection marker (Figure 5C). To confirm the CLIC/GEEC pathway involvement in the BKPyV *trans*-infection process, we finally tested the effect of the ciliobrevin D (CBD), a cytoplasmic dynein inhibitor(53), on MDDC during virus loading. Noticeably, a 50µM dose of CBD significantly decreased *trans*-infection with no measurable MDDC cytotoxicity (Figure 5D). Altogether, these results demonstrated that MDDC, while non-permissive to BKPyV, capture BKPyV virions and can transfer them to permissive cells like hRPTEC in a dynein-dependent manner.

Human MDDC are neither activated by BKPyV particles nor BKPyV-infected hRPTEC

MDDC can sense danger signals through various pattern-recognition receptors (PRR) including toll-like receptors (TLR) thus leading to MDDC maturation(54, 55). Conflicting results on DC activation by BKPyV in the literature prompted us to ask whether BKPyV attachment would lead to MDDC activation. Twenty-four hour MDDC cultures with VLP or virions were analyzed by flow cytometry to assess the acquisition or up-regulation of known DC maturation markers. A maturation enabling dose of LPS and R848(56), two TLR agonists, and a Modified Vaccinia Ankara (MVA) attenuated poxvirus known to activate MDDC were added as positive controls of maturation when necessary. First, expression of CD86, a sensitive and reliable marker of DC maturation (57), was assessed. Only exposure to TLR agonists or to the Modified Vaccinia Ankara attenuated poxvirus known to activate MDDC induced CD86 upregulation ((58-61); Figure 6A). Accordingly, no IL-12p70, a T helper type 1 cytokine, IL-10 or IL-8 were detected in MDDC culture supernatants cultivated with BKPyV (Figure 6B). Expression of the

bioRxiv preprint doi: https://doi.org/10.1101/2020.09.04.282426; this version posted September 4, 2020. The copyright holder for this preprint (which was not certified by peer review) is the author/funder, who has granted bioRxiv a license to display the preprint in perpetuity. It is made available under aCC-BY-NC-ND 4.0 International license.

CD80, CD83, CD40, CCR7 and HLA-DR on MDDC gave consistent results (Figure 6C). Then we hypothesized that MDDC could be activated not by BKPyV particles *per se* but by BKPyV-infected hRPTEC. HRPTEC infection was monitored by RT-qPCR for *LTAg* mRNA expression (data not shown). In that setting, MDDC CD86 expression did not vary upon cultivation with BKPyV-infected cells (Figure 6D). To exclude "under the radar" activation signals, we finally performed a digital RNA sequencing (DGEseq; REF) of BKPyV-infected MDDC compared to non-infected cells. In line with previous experiments, no difference was observed between BKPyV-infected and non-infected MDDC in terms of mRNA profile reprogramming at one dpi (Figure 6E). These results confirmed that MDDC were unresponsive to BKPyV and BKPyV-infected hRPTEC.

Internalized BKPyV is protected from neutralization

Together with cellular immune responses, neutralizing anti-BKPyV antibodies (NAbs) are required to control infection or reactivation in KTR(17, 62-66) and healthy donors(67). Here we wondered whether BKPyV could be protected from neutralization when internalized by MDDC. To address this point, *trans*-infection was performed in the presence of neutralizing and control sera from BKPyV reactivating or non-reactivating KTR respectively. Neutralizing antibodies completely blocked hRPTEC *cis*-infection whereas the control serum had no effect (Figure 7). When virions were pre-incubated with NAbs prior to MDDC loading, a significant loss in *trans*-infection was observed compared to controls. As a conclusion, NAbs were ineffective when used after BKPyV loading of MDDC suggesting virions were protected from neutralization once internalized.

bioRxiv preprint doi: https://doi.org/10.1101/2020.09.04.282426; this version posted September 4, 2020. The copyright holder for this preprint (which was not certified by peer review) is the author/funder, who has granted bioRxiv a license to display the preprint in perpetuity. It is made available under aCC-BY-NC-ND 4.0 International license.

Blood and kidney CD1c+ cDC display similar BKPyV *trans*-infection abilities and non-permissiveness to MDDC

MDDC were shown to be closely related to inflammatory DC in humans(68, 69) so to ensure our observations were not biased by the DC generation protocol, we first wondered whether cDC, the most abundant tissue and blood DC subset under non-inflammatory conditions, could behave like MDDC. First, VLP were incubated with whole blood of healthy volunteers and VLP staining was further analyzed by flow cytometry on both cDC (CD11c+) and plasmacytoid (pDC; CD123+) DC among HLA-DR$^+$ Lin$^-$ cells (Supplemental Figure 1). A significant proportion of cDC bound VLP whereas no binding was detected on pDC (Supplemental Figure 1 and Figure 8A). Importantly, binding to cDC was not affected by Fc receptor blockade suggesting that VLP attachment did not depend on anti-VP1 antibodies in whole blood of healthy donors (Figure 8B). To avoid any interference due to the whole blood environment, CD1c$^+$ DC, representing the main myeloid DC subset in blood(70) and kidney(71) were sorted according to the gating strategy displayed in Supplemental Figure 2, incubated with VLP and analyzed by flow cytometry. Blood and kidney CD1c$^+$ cDC were clearly capable of binding VLP as well as virions in a dose-dependent manner (Figures 8C and 8D, respectively). Then, we showed that like MDDC, CD1c+ cDC were unresponsive to BKPyV particles (Figure 8E). We finally demonstrated that sorted CD1c+ cDC enabled BKPyV *trans*-infection to permissive cells while being resistant to infection themselves (Figure 8F). Taken together our results demonstrate that biologically relevant blood and renal CD1c$^+$ cDC behave similarly to MDDC with respect to BKPyV infection.

Discussion

bioRxiv preprint doi: https://doi.org/10.1101/2020.09.04.282426; this version posted September 4, 2020. The copyright holder for this preprint (which was not certified by peer review) is the author/funder, who has granted bioRxiv a license to display the preprint in perpetuity. It is made available under aCC-BY-NC-ND 4.0 International license.

In this study, cDC, either generated *in vitro* or isolated from human blood and kidney, were shown to support BKPyV attachment in a sialic acid-dependent manner and subsequent clathrin-independent endocytosis through two distinct pathways, the first involving GRAF-1+ CLIC/GEEC and the second, minor pathway dependent on EEA1+ macropinocytic endocytosis. However, we did not provide evidence on potential spatio-temporal connections between both compartments. Upon contact, cDC were not activated by viral particles or BKPyV-infected cells. Moreover, we showed that MDDC and CD1c+ cDC were non-permissive to BKPyV infection. Internalized or membrane-bound BKPyV virions kept their ability to *trans*-infect permissive cells like hRPTEC and were also shown to be protected from neutralization by sera of BKPyV reactivating KTR.

We demonstrated that BKPyV interacts with human MDDC in a dose- and sialic acid-dependent manner suggesting these cells are equipped with BKPyV receptors, likely GD1b and GT1b(46). Upon attachment, BKPyV was shown to massively accumulate in pleiomorphous GRAF-1+ endocytic vesicles originating from the PM and partially overlapping with CTxB containing vesicles in MDDC. Although not proven here, it is tempting to speculate that a similar entry pathway for BKPyV occurs in CD1c-sorted cDC. This compartment was identified as CLIC/GEEC vesicles whose formation is clathrin-independent (see for review (72)). Interestingly, BKPyV was shown to infect hRPTEC in a clathrin- and caveolin-independent manner indicating that some BKPyV entry steps might be common between those cells and cDC(73, 74). Ewers and colleagues demonstrated that SV40 triggers the formation of PM invaginations related to CLIC/GEEC endocytosis after binding to GM1 in caveolin-1 deficient or energy-depleted cells(48). Multiple interactions between chemically defined GM1 PM clusters and SV40 capsomers were demonstrated to promote PM curvature and the formation of pleiomorphous tubules containing viral particles. CLIC/GEEC endocytosis has not been thoroughly documented for BKPyV before our results, even though Drachenberg et al

bioRxiv preprint doi: https://doi.org/10.1101/2020.09.04.282426; this version posted September 4, 2020. The copyright holder for this preprint (which was not certified by peer review) is the author/funder, who has granted bioRxiv a license to display the preprint in perpetuity. It is made available under aCC-BY-NC-ND 4.0 International license.

observed BKPyV virions within tubular structures in hRPTEC from PVAN biopsies(30). Whether these tubular vesicles result from early endocytosis or from viral progeny remains to be clarified. Although the microtubule-associated motor protein, dynein 1, was shown not to play a role in BKPyV(75), JCPyV and SV40 infection(76), here we demonstrated that a specific chemical inhibitor of the dynein protein family caused a measurable reduction of the *trans*-infection process by MDDC indicating distinct cell-specific requirements for BKPyV entry. After internalization, BKPyV(77), JCPyV(77, 78), SV40(77, 79) and MuPyV(80) were shown to reach the ER within the first ten hours after cell attachment to hRPTEC(46, 75). This step is crucial for the infection(46, 75, 81, 82) since it is followed by the release of partially uncoated virions in the cytosol and import of viral genomes to the nucleus to initiate replication. This question was not directly addressed in the present study but the absence of LTAg in MDDC after several days pi strongly suggests either BKPyV does not undergo uncoating or that the CLIC/GEEC endocytosis does not lead to productive infection. In non-immune cells, CLIC/GEEC was shown as the main productive AAV2 infection route, invalidating the second possibility(83). These discrepancies between our results and former studies might reflect multiple common as well as distinct BKPyV entry steps according to the cell type studied. Further work is needed to establish the molecular determinants of such differences between non-immune and immune cells like cDC. A recent review pointed out the link between the CLIC/GEEC endocytosis and glycosphingolipids (GSL) which encompass gangliosides in the establishment of cell polarity(72). DC polarization leading to the formation of a synapse is an important event in T cell priming (see for review(84)) but might also be crucial in the BKPyV *trans*-infection process we described here. GSL are known to form lipid rafts on the PM (see for review(85)). Such micro domains function as a platform to segregate a wide range of effector molecules including GPI-anchored cargos(86). Wang and colleagues demonstrated that GPI-anchored molecules, which utilize the CLIC/GEEC endocytic pathway upon ligand

bioRxiv preprint doi: https://doi.org/10.1101/2020.09.04.282426; this version posted September 4, 2020. The copyright holder for this preprint (which was not certified by peer review) is the author/funder, who has granted bioRxiv a license to display the preprint in perpetuity. It is made available under aCC-BY-NC-ND 4.0 International license.

409 binding, share biosynthetic pathways and common cellular locations with GSL(87). Such
410 findings could link the ganglioside-mediated BKPyV attachment to viral endocytosis even in
411 immune cells.

412 An important DC function is the ability to sense microbes through the recognition of conserved
413 pathogen-associated molecular patterns (PAMP) by PM-bound (toll-like and C-type lectin
414 receptors, TLR and CLR respectively), endosomal (TLR) or modified DNA/RNA cytoplasmic
415 receptors altogether termed PRR(88). Viral particles as supramolecular arrangements of
416 proteins and nucleic acids can be considered as PAMPs. Zepeda-Cervantes et al (Frontiers
417 Immunol, 2020) have recently discussed numerous examples of VLP sensing leading to
418 activation of human DC in a review(89). In contrast, both *in vitro*-generated murine and human
419 DC were shown to remain unresponsive to BK- and JCPyV VLP(23, 26). Our results with
420 human MDDC as well as freshly isolated blood and renal CD1c+ cDC confirm these
421 observations and extend them to *bona fide* DC subsets supporting that such an immune
422 ignorance towards BKPyV could exist *in vivo*. Two recent comprehensive studies demonstrated
423 that hRPTEC fail to sense BKPyV(90, 91). This was shown to be partly dependent on the
424 expression of the agnoprotein, a viral factor whose function has remained unclear so far(91).
425 While BKPyV escape mechanisms seem to depend on viral gene expression in hRPTEC, we
426 consider that different escape mechanisms are at work in BKPyV refractory cDC. The observed
427 accumulation of BKPyV into CLIC/GEEC vesicles in MDDC after two hours might lead to
428 their segregation in a PRR-free compartment. Unfortunately, whether PRR are present in the
429 CLIC/GEEC compartment is unknown.

430 We demonstrated that although renal CD1c+ DC are refractory to BKPyV infection they remain
431 able to capture virions and *trans*-infect hRPTEC *in vitro*. CD1c+ DC are normally present in
432 the human renal interstitium surrounding the proximal tubules and glomeruli(29, 34, 71) but in
433 PVAN lesions, a significant increase in infiltrating CD1c+ DC is documented(34). Whether the

bioRxiv preprint doi: https://doi.org/10.1101/2020.09.04.282426; this version posted September 4, 2020. The copyright holder for this preprint (which was not certified by peer review) is the author/funder, who has granted bioRxiv a license to display the preprint in perpetuity. It is made available under aCC-BY-NC-ND 4.0 International license.

CD1c+ DC infiltrate has a key role in viral spreading *in vivo* deserves to be investigated through combined multidimensional imaging techniques and spatial RNA/DNA sequencing. Upon inflammation, monocytes are recruited in tissues where they differentiate in inflammatory DC with transcriptomic profiles closely related to those observed in MDDC(68, 69). PVAN develops in an inflammatory context. Therefore, it is tempting to speculate that along with resident CD1c+ DC, inflammatory DC could participate in the potentiation of BKPyV infection.

In this study, we demonstrated that cDC, namely MDDC and blood or kidney CD1c+ resident DC can capture infectious BKPyV through an unprecedented endocytic pathway in cDC and for BKPyV, and transfer the virus to permissive cells like hRPTEC without DC activation or infection, suggesting a role for cDC in BKPyV spreading. Moreover, we showed that internalized virions were protected from neutralization by serum from KTR. Taken together our results support the idea that cDC could facilitate BKPyV infection by favoring its spreading and limiting specific T lymphocyte activation due to the cDC ignorance towards BKPyV antigens and the circumvention of neutralization by specific antibodies. Hence, this work could help to understand how cDC could aggravate BKPyV infection in KTR.

Author contributions

M.S. and F.H. designed, performed, analyzed and interpreted all experiments exept RNAseq data and wrote the paper. F.C., C.P., C.B., A.G., S.N., P.H., J.V., N.M., J.D., P.G., J.B.-G. performed and analyzed experiments. K.R., C.K.-A. and J.B. collected and characterized all human samples used in this study. A.T., R.J., D.McI. and C.B.-B. participated in experimental design and data discussion and actively contributed to the manuscript preparation. M.G.

bioRxiv preprint doi: https://doi.org/10.1101/2020.09.04.282426; this version posted September 4, 2020. The copyright holder for this preprint (which was not certified by peer review) is the author/funder, who has granted bioRxiv a license to display the preprint in perpetuity. It is made available under aCC-BY-NC-ND 4.0 International license.

457 analyzed RNAseq data and deposited datasets on appropriate databases. F.H. supervised this
458 study. All authors reviewed and approved the manuscript.

459

460 ## Acknowledgments and financial disclosures

461 The authors would like to thank Camille Roesch (Izon Sciences Europe Ltd.) for her help in the
462 VLP and BKPyV particle titrations based on the TRPS technique and Hélène Roux and Felix
463 Letertre for their technical assistance. This work was supported by the Fondation d'Entreprises
464 Progreffe (Mathieu Sikorski's salary). This work was carried out in the context of the IHU-
465 Cesti project, which received French government financial support managed by the Agence
466 Nationale de la Recherche via the ''Investment into the Future'' program ANR-10-IBHU-005.
467 The IHU- Cesti project is also supported by Nantes Metropole and the Pays de la Loire Region.
468 The authors declare no conflict of interest. The funders had no role in study design, data
469 collection and analysis, decision to publish, or preparation of the manuscript.

470

471 **References**

472 1. Gardner SD, Field AM, Coleman DV, Hulme B. New human papovavirus (B.K.)
473 isolated from urine after renal transplantation. Lancet. 1971.
474 2. Seif I, Khoury G, Dhar R. The genome of human papovavirus BKV. Cell. 1979
475 Dec;18(4):963-77. PubMed PMID: 229976.
476 3. Wright PJ, Di Mayorca G. Virion polypeptide composition of the human papovavirus
477 BK: comparison with simian virus 40 and polyoma virus. J Virol. 1975 Apr;15(4):828-35.
478 PubMed PMID: 163921. Pubmed Central PMCID: 354526.

bioRxiv preprint doi: https://doi.org/10.1101/2020.09.04.282426; this version posted September 4, 2020. The copyright holder for this preprint (which was not certified by peer review) is the author/funder, who has granted bioRxiv a license to display the preprint in perpetuity. It is made available under aCC-BY-NC-ND 4.0 International license.

479 4. Chesters PM, Heritage J, McCance DJ. Persistence of DNA sequences of BK virus and
480 JC virus in normal human tissues and in diseased tissues. J Infect Dis. 1983 Apr;147(4):676-
481 84. PubMed PMID: 6302172.
482 5. Egli A, Infanti L, Dumoulin A, Buser A, Samaridis J, Stebler C, et al. Prevalence of
483 polyomavirus BK and JC infection and replication in 400 healthy blood donors. J Infect Dis.
484 2009 Mar 15;199(6):837-46. PubMed PMID: 19434930.
485 6. Brown P, Tsai T, Gajdusek DC. Seroepidemiology of human papovaviruses. Discovery
486 of virgin populations and some unusual patterns of antibody prevalence among remote peoples
487 of the world. American journal of epidemiology. 1975 Oct;102(4):331-40. PubMed PMID:
488 233851.
489 7. Flaegstad T, Traavik T, Kristiansen BE. Age-dependent prevalence of BK virus IgG and
490 IgM antibodies measured by enzyme-linked immunosorbent assays (ELISA). The Journal of
491 hygiene. 1986 Jun;96(3):523-8. PubMed PMID: 3016078. Pubmed Central PMCID: 2129697.
492 8. Heritage J, Chesters PM, McCance DJ. The persistence of papovavirus BK DNA
493 sequences in normal human renal tissue. Journal of Medical Virology. 1981;8(2):143-50. en.
494 9. Cesaro S, Facchin C, Tridello G, Messina C, Calore E, Biasolo MA, et al. A prospective
495 study of BK-virus-associated haemorrhagic cystitis in paediatric patients undergoing allogeneic
496 haematopoietic stem cell transplantation. Bone marrow transplantation. 2008 Feb;41(4):363-
497 70. PubMed PMID: 17982496.
498 10. Erard V, Storer B, Corey L, Nollkamper J, Huang ML, Limaye A, et al. BK virus
499 infection in hematopoietic stem cell transplant recipients: frequency, risk factors, and
500 association with postengraftment hemorrhagic cystitis. Clinical infectious diseases : an official
501 publication of the Infectious Diseases Society of America. 2004 Dec 15;39(12):1861-5.
502 PubMed PMID: 15578413.

bioRxiv preprint doi: https://doi.org/10.1101/2020.09.04.282426; this version posted September 4, 2020. The copyright holder for this preprint (which was not certified by peer review) is the author/funder, who has granted bioRxiv a license to display the preprint in perpetuity. It is made available under aCC-BY-NC-ND 4.0 International license.

503 11. Hirsch HH. Polyomavirus BK Nephropathy: A (Re-)emerging Complication in Renal
504 Transplantation. American Journal of Transplantation. 2002;2(1):25-30. en.
505 12. Leung AY, Suen CK, Lie AK, Liang RH, Yuen KY, Kwong YL. Quantification of
506 polyoma BK viruria in hemorrhagic cystitis complicating bone marrow transplantation. Blood.
507 2001 Sep 15;98(6):1971-8. PubMed PMID: 11535537.
508 13. Bicalho CS, Oliveira RDR, David DR, Fink M, Agena F, Castro MC, et al.
509 Determination of viremia cut-off for risk to develop BKPyV-associated nephropathy among
510 kidney transplant recipients. Transplant infectious disease : an official journal of the
511 Transplantation Society. 2018 Oct;20(5):e12969. PubMed PMID: 30074295.
512 14. Pollara CP, Corbellini S, Chiappini S, Sandrini S, De Tomasi D, Bonfanti C, et al.
513 Quantitative viral load measurement for BKV infection in renal transplant recipients as a
514 predictive tool for BKVAN. The new microbiologica. 2011 Apr;34(2):165-71. PubMed PMID:
515 21617828.
516 15. Randhawa P, Ho A, Shapiro R, Vats A, Swalsky P, Finkelstein S, et al. Correlates of
517 quantitative measurement of BK polyomavirus (BKV) DNA with clinical course of BKV
518 infection in renal transplant patients. Journal of clinical microbiology. 2004 Mar;42(3):1176-
519 80. PubMed PMID: 15004071. Pubmed Central PMCID: 356850.
520 16. Randhawa PS, Finkelstein S, Scantlebury V, Shapiro R, Vivas C, Jordan M, et al.
521 Human polyoma virus-associated interstitial nephritis in the allograft kidney. Transplantation.
522 1999;67(1):103-9. PubMed PMID: 9921805. English.
523 17. Binggeli S, Egli A, Schaub S, Binet I, Mayr M, Steiger J, et al. Polyomavirus BK-
524 specific cellular immune response to VP1 and large T-antigen in kidney transplant recipients.
525 American journal of transplantation : official journal of the American Society of
526 Transplantation and the American Society of Transplant Surgeons. 2007 May;7(5):1131-9.
527 PubMed PMID: 17359507.

bioRxiv preprint doi: https://doi.org/10.1101/2020.09.04.282426; this version posted September 4, 2020. The copyright holder for this preprint (which was not certified by peer review) is the author/funder, who has granted bioRxiv a license to display the preprint in perpetuity. It is made available under aCC-BY-NC-ND 4.0 International license.

528 18. Leboeuf C, Wilk S, Achermann R, Binet I, Golshayan D, Hadaya K, et al. BK
529 Polyomavirus-Specific 9mer CD8 T Cell Responses Correlate With Clearance of BK Viremia
530 in Kidney Transplant Recipients: First Report From the Swiss Transplant Cohort Study.
531 American journal of transplantation : official journal of the American Society of
532 Transplantation and the American Society of Transplant Surgeons. 2017 Oct;17(10):2591-600.
533 PubMed PMID: 28326672.
534 19. Li J, Melenhorst J, Hensel N, Rezvani K, Sconocchia G, Kilical Y, et al. T-cell responses
535 to peptide fragments of the BK virus T antigen: implications for cross-reactivity of immune
536 response to JC virus. The Journal of general virology. 2006 Oct;87(Pt 10):2951-60. PubMed
537 PMID: 16963754.
538 20. Mutlu E, Koksoy S, Mutlu D, Yilmaz VT, Kocak H, Dinckan A, et al. Quantitative
539 analysis of BKV-specific CD4+ T cells before and after kidney transplantation. Transplant
540 immunology. 2015 Sep;33(1):20-6. PubMed PMID: 26048051.
541 21. Lamarche C, Orio J, Georges-Tobar V, Pincez T, Goupil M, Dahmani A, et al. Clinical-
542 Scale Rapid Autologous BK Virus-Specific T Cell Line Generation From Kidney Transplant
543 Recipients With Active Viremia for Adoptive Immunotherapy. Transplantation. 2017
544 Nov;101(11):2713-21. PubMed PMID: 28230645.
545 22. Drake III DR, Shawver ML, Hadley A, Butz E, Maliszewski C, Lukacher AE. Induction
546 of Polyomavirus-Specific CD8+T Lymphocytes by Distinct Dendritic Cell Subpopulations.
547 Journal of Virology. 2001 2001-01-01. en.
548 23. Lenz P, Day PM, Pang YY, Frye SA, Jensen PN, Lowy DR, et al. Papillomavirus-like
549 particles induce acute activation of dendritic cells. Journal of immunology. 2001 May
550 1;166(9):5346-55. PubMed PMID: 11313370.
551 24. Gedvilaite A, Kucinskaite-Kodze I, Lasickiene R, Timinskas A, Vaitiekaite A, Ziogiene
552 D, et al. Evaluation of Trichodysplasia Spinulosa-Associated Polyomavirus Capsid Protein as

bioRxiv preprint doi: https://doi.org/10.1101/2020.09.04.282426; this version posted September 4, 2020. The copyright holder for this preprint (which was not certified by peer review) is the author/funder, who has granted bioRxiv a license to display the preprint in perpetuity. It is made available under aCC-BY-NC-ND 4.0 International license.

553 a New Carrier for Construction of Chimeric Virus-Like Particles Harboring Foreign Epitopes.
554 Viruses. 2015 Jul 29;7(8):4204-29. PubMed PMID: 26230706. Pubmed Central PMCID:
555 4576179.
556 25. Changyong C, Sun M, Li H, Brockmeyer N, Wu NP. Simian virus 40 inhibits
557 differentiation and maturation of rhesus macaque DC-SIGN(+) dendritic cells. Eur J Med Res.
558 2010 Sep 24;15(9):377-82. PubMed PMID: 20952346. Pubmed Central PMCID: 3351904.
559 26. Gedvilaite A, Dorn DC, Sasnauskas K, Pecher G, Bulavaite A, Lawatscheck R, et al.
560 Virus-like particles derived from major capsid protein VP1 of different polyomaviruses differ
561 in their ability to induce maturation in human dendritic cells. Virology. 2006;354(2):252-60.
562 27. Comoli P, Basso S, Azzi A, Moretta A, De Santis R, Del Galdo F, et al. Dendritic cells
563 pulsed with polyomavirus BK antigen induce ex vivo polyoma BK virus-specific cytotoxic T-
564 cell lines in seropositive healthy individuals and renal transplant recipients. Journal of the
565 American Society of Nephrology : JASN. 2003 Dec;14(12):3197-204. PubMed PMID:
566 14638918.
567 28. Kaur A, Wilhelm M, Wilk S, Hirsch HH. BK polyomavirus-specific antibody and T-
568 cell responses in kidney transplantation: update. Current opinion in infectious diseases. 2019
569 Dec;32(6):575-83. PubMed PMID: 31567736.
570 29. Woltman AM, de Fijter JW, Zuidwijk K, Vlug AG, Bajema IM, van der Kooij SW, et
571 al. Quantification of dendritic cell subsets in human renal tissue under normal and pathological
572 conditions. Kidney International. 2007;71(10):1001-8.
573 30. Drachenberg CB, Papadimitriou JC, Wali R, Cubitt CL, Ramos E. BK Polyoma Virus
574 Allograft Nephropathy: Ultrastructural Features from Viral Cell Entry to Lysis. American
575 Journal of Transplantation. 2003;3(11):1383-92. en.
576 31. Kassianos AJ, Sampangi S, Wang X, Roper KE, Beagley K, Healy H, et al. Human
577 proximal tubule epithelial cells modulate autologous dendritic cell function. Nephrology,

bioRxiv preprint doi: https://doi.org/10.1101/2020.09.04.282426; this version posted September 4, 2020. The copyright holder for this preprint (which was not certified by peer review) is the author/funder, who has granted bioRxiv a license to display the preprint in perpetuity. It is made available under aCC-BY-NC-ND 4.0 International license.

578 dialysis, transplantation : official publication of the European Dialysis and Transplant
579 Association - European Renal Association. 2013 Feb;28(2):303-12. PubMed PMID: 22610986.
580 32. Kassianos AJ, Wang X, Sampangi S, Afrin S, Wilkinson R, Healy H. Fractalkine–
581 CX3CR1-dependent recruitment and retention of human CD1c+ myeloid dendritic cells by in
582 vitro–activated proximal tubular epithelial cells. Kidney International. 2015;87(6):1153-63.
583 33. Sampangi S, Kassianos AJ, Wang X, Beagley KW, Klein T, Afrin S, et al. The
584 Mechanisms of Human Renal Epithelial Cell Modulation of Autologous Dendritic Cell
585 Phenotype and Function. PLoS One. 2015;10(7):e0134688. PubMed PMID: 26230727.
586 Pubmed Central PMCID: 4521940.
587 34. Yapici U, Kers J, Slavujevic-Letic I, Stokman G, Roelofs JJTH, van Aalderen MC, et
588 al. Intragraft Blood Dendritic Cell Antigen-1-Positive Myeloid Dendritic Cells Increase during
589 BK Polyomavirus-Associated Nephropathy. Journal of the American Society of Nephrology.
590 2015;27(8):2502-10.
591 35. Hirsch HH, Randhawa P. BK Polyomavirus in Solid Organ Transplantation. American
592 Journal of Transplantation. 2013;13(s4):179-88. en.
593 36. Kuypers DR. Management of polyomavirus-associated nephropathy in renal transplant
594 recipients. Nature reviews Nephrology. 2012 Apr 17;8(7):390-402. PubMed PMID: 22508181.
595 37. Sallusto F, Lanzavecchia A. Efficient presentation of soluble antigen by cultured human
596 dendritic cells is maintained by granulocyte/macrophage colony-stimulating factor plus
597 interleukin 4 and downregulated by tumor necrosis factor alpha. J Exp Med. 1994 Apr
598 01;179(4):1109-18. PubMed PMID: 8145033. Pubmed Central PMCID: 2191432.
599 38. Pastrana DV, Ray U, Magaldi TG, Schowalter RM, Cuburu N, Buck CB. BK
600 polyomavirus genotypes represent distinct serotypes with distinct entry tropism. J Virol. 2013
601 Sep;87(18):10105-13. PubMed PMID: 23843634. Pubmed Central PMCID: 3754014.

bioRxiv preprint doi: https://doi.org/10.1101/2020.09.04.282426; this version posted September 4, 2020. The copyright holder for this preprint (which was not certified by peer review) is the author/funder, who has granted bioRxiv a license to display the preprint in perpetuity. It is made available under aCC-BY-NC-ND 4.0 International license.

602 39. Moriyama T, Sorokin A. BK virus (BKV): infection, propagation, quantitation,
603 purification, labeling, and analysis of cell entry. Current protocols in cell biology. 2009
604 Mar;Chapter 26:Unit 26 2. PubMed PMID: 19283732. Pubmed Central PMCID: 2818100.
605 40. Pastrana DV, Brennan DC, Cuburu N, Storch GA, Viscidi RP, Randhawa PS, et al.
606 Neutralization serotyping of BK polyomavirus infection in kidney transplant recipients. PLoS
607 pathogens. 2012;8(4):e1002650. PubMed PMID: 22511874. Pubmed Central PMCID:
608 3325208.
609 41. Halary F, Amara A, Lortat-Jacob H, Messerle M, Delaunay T, Houlès C, et al. Human
610 Cytomegalovirus Binding to DC-SIGN Is Required for Dendritic Cell Infection and Target Cell
611 trans-Infection. Immunity. 2002;17(5):653-64.
612 42. Haspot F, Lavault A, Sinzger C, Laib Sampaio K, Stierhof Y-D, Pilet P, et al. Human
613 Cytomegalovirus Entry into Dendritic Cells Occurs via a Macropinocytosis-Like Pathway in a
614 pH-Independent and Cholesterol-Dependent Manner. PLoS ONE. 2012;7(4):e34795.
615 43. Kilens S, Meistermann D, Moreno D, Chariau C, Gaignerie A, Reignier A, et al. Parallel
616 derivation of isogenic human primed and naive induced pluripotent stem cells. Nature
617 communications. 2018 Jan 24;9(1):360. PubMed PMID: 29367672. Pubmed Central PMCID:
618 5783949.
619 44. Touze A, Bousarghin L, Ster C, Combita AL, Roingeard P, Coursaget P. Gene transfer
620 using human polyomavirus BK virus-like particles expressed in insect cells. The Journal of
621 general virology. 2001 Dec;82(Pt 12):3005-9. PubMed PMID: 11714977.
622 45. Touze A, Gaitan J, Arnold F, Cazal R, Fleury MJ, Combelas N, et al. Generation of
623 Merkel cell polyomavirus (MCV)-like particles and their application to detection of MCV
624 antibodies. Journal of clinical microbiology. 2010 May;48(5):1767-70. PubMed PMID:
625 20181914. Pubmed Central PMCID: 2863896.

bioRxiv preprint doi: https://doi.org/10.1101/2020.09.04.282426; this version posted September 4, 2020. The copyright holder for this preprint (which was not certified by peer review) is the author/funder, who has granted bioRxiv a license to display the preprint in perpetuity. It is made available under aCC-BY-NC-ND 4.0 International license.

626 46. Low JA, Magnuson B, Tsai B, Imperiale MJ. Identification of Gangliosides GD1b and
627 GT1b as Receptors for BK Virus. Journal of Virology. 2006;80(3):1361-6.
628 47. Sharma PM, Gupta G, Vats A, Shapiro R, Randhawa P. Phylogenetic analysis of
629 polyomavirus BK sequences. J Virol. 2006 Sep;80(18):8869-79. PubMed PMID: 16940499.
630 Pubmed Central PMCID: 1563921.
631 48. Ewers H, Romer W, Smith AE, Bacia K, Dmitrieff S, Chai W, et al. GM1 structure
632 determines SV40-induced membrane invagination and infection. Nat Cell Biol. 2010
633 Jan;12(1):11-8; sup pp 1-2. PubMed PMID: 20023649.
634 49. Kirkham M, Fujita A, Chadda R, Nixon SJ, Kurzchalia TV, Sharma DK, et al.
635 Ultrastructural identification of uncoated caveolin-independent early endocytic vehicles. The
636 Journal of cell biology. 2005 Jan 31;168(3):465-76. PubMed PMID: 15668297. Pubmed
637 Central PMCID: 2171740.
638 50. Sabharanjak S, Sharma P, Parton RG, Mayor S. GPI-anchored proteins are delivered to
639 recycling endosomes via a distinct cdc42-regulated, clathrin-independent pinocytic pathway.
640 Developmental cell. 2002 Apr;2(4):411-23. PubMed PMID: 11970892.
641 51. Lundmark R, Doherty GJ, Howes MT, Cortese K, Vallis Y, Parton RG, et al. The
642 GTPase-activating protein GRAF1 regulates the CLIC/GEEC endocytic pathway. Current
643 biology : CB. 2008 Nov 25;18(22):1802-8. PubMed PMID: 19036340. Pubmed Central
644 PMCID: 2726289.
645 52. Cheneau C, Coulon F, Porkolab V, Fieschi F, Laurant S, Razanajaona-Doll D, et al. Fine
646 Mapping the Interaction Between Dendritic Cell-Specific Intercellular Adhesion Molecule
647 (ICAM)-3-Grabbing Nonintegrin and the Cytomegalovirus Envelope Glycoprotein B. J Infect
648 Dis. 2018 Jul 2;218(3):490-503. PubMed PMID: 29648611. Pubmed Central PMCID:
649 6049025.

bioRxiv preprint doi: https://doi.org/10.1101/2020.09.04.282426; this version posted September 4, 2020. The copyright holder for this preprint (which was not certified by peer review) is the author/funder, who has granted bioRxiv a license to display the preprint in perpetuity. It is made available under aCC-BY-NC-ND 4.0 International license.

650 53. Ye Y, Meyer HH, Rapoport TA. The AAA ATPase Cdc48/p97 and its partners transport
651 proteins from the ER into the cytosol. Nature. 2001 Dec 6;414(6864):652-6. PubMed PMID:
652 11740563.
653 54. Du J, Wu Z, Ren S, Wei Y, Gao M, Randolph GJ, et al. TLR8 agonists stimulate newly
654 recruited monocyte-derived cells into potent APCs that enhance HBsAg immunogenicity.
655 Vaccine. 2010 Aug 31;28(38):6273-81. PubMed PMID: 20637759. Pubmed Central PMCID:
656 3031106.
657 55. Thoma-Uszynski S, Kiertscher SM, Ochoa MT, Bouis DA, Norgard MV, Miyake K, et
658 al. Activation of toll-like receptor 2 on human dendritic cells triggers induction of IL-12, but
659 not IL-10. Journal of immunology. 2000 Oct 1;165(7):3804-10. PubMed PMID: 11034386.
660 56. Picarda G, Cheneau C, Humbert JM, Beriou G, Pilet P, Martin J, et al. Functional
661 Langerinhigh-Expressing Langerhans-like Cells Can Arise from CD14highCD16- Human
662 Blood Monocytes in Serum-Free Condition. Journal of immunology. 2016 May 1;196(9):3716-
663 28. PubMed PMID: 27016604.
664 57. Manel N, Hogstad B, Wang Y, Levy DE, Unutmaz D, Littman DR. A cryptic sensor for
665 HIV-1 activates antiviral innate immunity in dendritic cells. Nature. 2010;467(7312):214-7.
666 58. Drillien R, Spehner D, Hanau D. Modified vaccinia virus Ankara induces moderate
667 activation of human dendritic cells. The Journal of general virology. 2004 Aug;85(Pt 8):2167-
668 75. PubMed PMID: 15269355.
669 59. Pascutti MF, Rodriguez AM, Falivene J, Giavedoni L, Drexler I, Gherardi MM.
670 Interplay between modified vaccinia virus Ankara and dendritic cells: phenotypic and
671 functional maturation of bystander dendritic cells. J Virol. 2011 Jun;85(11):5532-45. PubMed
672 PMID: 21411535. Pubmed Central PMCID: 3094969.

bioRxiv preprint doi: https://doi.org/10.1101/2020.09.04.282426; this version posted September 4, 2020. The copyright holder for this preprint (which was not certified by peer review) is the author/funder, who has granted bioRxiv a license to display the preprint in perpetuity. It is made available under aCC-BY-NC-ND 4.0 International license.

673 60. Tao R, Li L, Huang W, Zheng L. Activation of human dendritic cells by recombinant
674 modified vaccinia virus Ankara vectors encoding survivin and IL-2 genes in vitro. Human gene
675 therapy. 2010 Jan;21(1):98-108. PubMed PMID: 19715401.
676 61. Trevor KT, Hersh EM, Brailey J, Balloul JM, Acres B. Transduction of human dendritic
677 cells with a recombinant modified vaccinia Ankara virus encoding MUC1 and IL-2. Cancer
678 immunology, immunotherapy : CII. 2001 Oct;50(8):397-407. PubMed PMID: 11726134.
679 62. Bohl DL, Brennan DC, Ryschkewitsch C, Gaudreault-Keener M, Major EO, Storch GA.
680 BK virus antibody titers and intensity of infections after renal transplantation. Journal of clinical
681 virology : the official publication of the Pan American Society for Clinical Virology. 2008
682 Oct;43(2):184-9. PubMed PMID: 18676176. Pubmed Central PMCID: 2701220.
683 63. Chen Y, Trofe J, Gordon J, Du Pasquier RA, Roy-Chaudhury P, Kuroda MJ, et al.
684 Interplay of cellular and humoral immune responses against BK virus in kidney transplant
685 recipients with polyomavirus nephropathy. J Virol. 2006 Apr;80(7):3495-505. PubMed PMID:
686 16537617. Pubmed Central PMCID: 1440396.
687 64. Comoli P, Azzi A, Maccario R, Basso S, Botti G, Basile G, et al. Polyomavirus BK-
688 specific immunity after kidney transplantation. Transplantation. 2004 Oct 27;78(8):1229-32.
689 PubMed PMID: 15502726.
690 65. Randhawa PS, Gupta G, Vats A, Shapiro R, Viscidi RP. Immunoglobulin G, A, and M
691 responses to BK virus in renal transplantation. Clinical and vaccine immunology : CVI. 2006
692 Sep;13(9):1057-63. PubMed PMID: 16960119. Pubmed Central PMCID: 1563576.
693 66. Schachtner T, Muller K, Stein M, Diezemann C, Sefrin A, Babel N, et al. BK virus-
694 specific immunity kinetics: a predictor of recovery from polyomavirus BK-associated
695 nephropathy. American journal of transplantation : official journal of the American Society of
696 Transplantation and the American Society of Transplant Surgeons. 2011 Nov;11(11):2443-52.
697 PubMed PMID: 21831150.

bioRxiv preprint doi: https://doi.org/10.1101/2020.09.04.282426; this version posted September 4, 2020. The copyright holder for this preprint (which was not certified by peer review) is the author/funder, who has granted bioRxiv a license to display the preprint in perpetuity. It is made available under aCC-BY-NC-ND 4.0 International license.

698 67. Lindner JM, Cornacchione V, Sathe A, Be C, Srinivas H, Riquet E, et al. Human
699 Memory B Cells Harbor Diverse Cross-Neutralizing Antibodies against BK and JC
700 Polyomaviruses. Immunity. 2019 Mar 19;50(3):668-76 e5. PubMed PMID: 30824324.
701 68. Goudot C, Coillard A, Villani AC, Gueguen P, Cros A, Sarkizova S, et al. Aryl
702 Hydrocarbon Receptor Controls Monocyte Differentiation into Dendritic Cells versus
703 Macrophages. Immunity. 2017 Sep 19;47(3):582-96 e6. PubMed PMID: 28930664.
704 69. Segura E, Touzot M, Bohineust A, Cappuccio A, Chiocchia G, Hosmalin A, et al.
705 Human inflammatory dendritic cells induce Th17 cell differentiation. Immunity. 2013 Feb
706 21;38(2):336-48. PubMed PMID: 23352235.
707 70. MacDonald KP, Munster DJ, Clark GJ, Dzionek A, Schmitz J, Hart DN.
708 Characterization of human blood dendritic cell subsets. Blood. 2002 Dec 15;100(13):4512-20.
709 PubMed PMID: 12393628.
710 71. Zuidwijk K, de Fijter JW, Mallat MJK, Eikmans M, van Groningen MC, Goemaere NN,
711 et al. Increased influx of myeloid dendritic cells during acute rejection is associated with
712 interstitial fibrosis and tubular atrophy and predicts poor outcome. Kidney International.
713 2012;81(1):64-75.
714 72. Shafaq-Zadah M, Dransart E, Johannes L. Clathrin-independent endocytosis, retrograde
715 trafficking, and cell polarity. Current opinion in cell biology. 2020 Jul 17;65:112-21. PubMed
716 PMID: 32688213.
717 73. Moriyama T, Marquez JP, Tetsuro W, Andrey S. Caveolar Endocytosis Is Critical for
718 BK Virus Infection of Human Renal Proximal Tubular Epithelial Cells. Journal of Virology.
719 2007 2007-08-15. en.
720 74. Zhao L, Marciano AT, Rivet CR, Imperiale MJ. Caveolin- and clathrin-independent
721 entry of BKPyV into primary human proximal tubule epithelial cells. Virology. 2016;492:66-
722 72.

bioRxiv preprint doi: https://doi.org/10.1101/2020.09.04.282426; this version posted September 4, 2020. The copyright holder for this preprint (which was not certified by peer review) is the author/funder, who has granted bioRxiv a license to display the preprint in perpetuity. It is made available under aCC-BY-NC-ND 4.0 International license.

723 75. Moriyama T, Sorokin A. Intracellular trafficking pathway of BK Virus in human renal
724 proximal tubular epithelial cells. Virology. 2008 Feb 20;371(2):336-49. PubMed PMID:
725 17976677. Pubmed Central PMCID: 2674336.
726 76. Ashok A, Atwood WJ. Contrasting roles of endosomal pH and the cytoskeleton in
727 infection of human glial cells by JC virus and simian virus 40. J Virol. 2003 Jan;77(2):1347-
728 56. PubMed PMID: 12502851. Pubmed Central PMCID: 140837.
729 77. Nelson CD, Carney DW, Derdowski A, Lipovsky A, Gee GV, O'Hara B, et al. A
730 retrograde trafficking inhibitor of ricin and Shiga-like toxins inhibits infection of cells by
731 human and monkey polyomaviruses. mBio. 2013 Nov 12;4(6):e00729-13. PubMed PMID:
732 24222489. Pubmed Central PMCID: 3892778.
733 78. Nelson CD, Stroh LJ, Gee GV, O'Hara BA, Stehle T, Atwood WJ. Modulation of a pore
734 in the capsid of JC polyomavirus reduces infectivity and prevents exposure of the minor capsid
735 proteins. J Virol. 2015 Apr;89(7):3910-21. PubMed PMID: 25609820. Pubmed Central
736 PMCID: 4403419.
737 79. Norkin LC, Anderson HA, Wolfrom SA, Oppenheim A. Caveolar endocytosis of simian
738 virus 40 is followed by brefeldin A-sensitive transport to the endoplasmic reticulum, where the
739 virus disassembles. J Virol. 2002 May;76(10):5156-66. PubMed PMID: 11967331. Pubmed
740 Central PMCID: 136127.
741 80. Maru S, Jin G, Desai D, Amin S, Shwetank, Lauver MD, et al. Inhibition of Retrograde
742 Transport Limits Polyomavirus Infection In Vivo. mSphere. 2017 Nov-Dec;2(6). PubMed
743 PMID: 29152583. Pubmed Central PMCID: 5687923.
744 81. Bennett SM, Jiang M, Imperiale MJ. Role of cell-type-specific endoplasmic reticulum-
745 associated degradation in polyomavirus trafficking. J Virol. 2013 Aug;87(16):8843-52.
746 PubMed PMID: 23740996. Pubmed Central PMCID: 3754070.

bioRxiv preprint doi: https://doi.org/10.1101/2020.09.04.282426; this version posted September 4, 2020. The copyright holder for this preprint (which was not certified by peer review) is the author/funder, who has granted bioRxiv a license to display the preprint in perpetuity. It is made available under aCC-BY-NC-ND 4.0 International license.

747 82. Jiang M, Abend JR, Tsai B, Imperiale MJ. Early Events during BK Virus Entry and
748 Disassembly. Journal of Virology. 2008;83(3):1350-8.
749 83. Nonnenmacher M, Weber T. Adeno-associated virus 2 infection requires endocytosis
750 through the CLIC/GEEC pathway. Cell host & microbe. 2011 Dec 15;10(6):563-76. PubMed
751 PMID: 22177561. Pubmed Central PMCID: 3257174.
752 84. Benvenuti F. The Dendritic Cell Synapse: A Life Dedicated to T Cell Activation.
753 Frontiers in immunology. 2016;7:70. PubMed PMID: 27014259. Pubmed Central PMCID:
754 4780025.
755 85. Gupta G, Surolia A. Glycosphingolipids in microdomain formation and their spatial
756 organization. FEBS letters. 2010 May 3;584(9):1634-41. PubMed PMID: 19941856.
757 86. Brown DA, London E. Structure and origin of ordered lipid domains in biological
758 membranes. The Journal of membrane biology. 1998 Jul 15;164(2):103-14. PubMed PMID:
759 9662555.
760 87. Wang Y, Maeda Y, Liu YS, Takada Y, Ninomiya A, Hirata T, et al. Cross-talks of
761 glycosylphosphatidylinositol biosynthesis with glycosphingolipid biosynthesis and ER-
762 associated degradation. Nature communications. 2020 Feb 13;11(1):860. PubMed PMID:
763 32054864. Pubmed Central PMCID: 7018848.
764 88. Iwasaki A, Medzhitov R. Control of adaptive immunity by the innate immune system.
765 Nature immunology. 2015 Apr;16(4):343-53. PubMed PMID: 25789684. Pubmed Central
766 PMCID: 4507498.
767 89. Zepeda-Cervantes J, Ramirez-Jarquin JO, Vaca L. Interaction Between Virus-Like
768 Particles (VLPs) and Pattern Recognition Receptors (PRRs) From Dendritic Cells (DCs):
769 Toward Better Engineering of VLPs. Frontiers in immunology. 2020;11:1100. PubMed PMID:
770 32582186. Pubmed Central PMCID: 7297083.

bioRxiv preprint doi: https://doi.org/10.1101/2020.09.04.282426; this version posted September 4, 2020. The copyright holder for this preprint (which was not certified by peer review) is the author/funder, who has granted bioRxiv a license to display the preprint in perpetuity. It is made available under aCC-BY-NC-ND 4.0 International license.

90. Caller LG, Davies CTR, Antrobus R, Lehner PJ, Weekes MP, Crump CM. Temporal Proteomic Analysis of BK Polyomavirus Infection Reveals Virus-Induced G2 Arrest and Highly Effective Evasion of Innate Immune Sensing. J Virol. 2019 Aug 15;93(16). PubMed PMID: 31142673. Pubmed Central PMCID: 6675895.

91. Manzetti J, Weissbach FH, Graf FE, Unterstab G, Wernli M, Hopfer H, et al. BK Polyomavirus Evades Innate Immune Sensing by Disrupting the Mitochondrial Network and Promotes Mitophagy. iScience. 2020 Jul 24;23(7):101257. PubMed PMID: 32599557. Pubmed Central PMCID: 7326741.

Figure legends

Figure 1: MDDC bind BKPyV particles in a dose- and sialic acid-dependent manner. (A) Negative contrast TEM picture of genotype Ib2 (gIb2) VLP. A 200nm scale bar is represented on the micrograph. (B) Fluorescent-labelled gIb2 VLP binding to hRPTEC, HEK293TT, MDDC and LNCaP (n=3) assessed by flow cytometry. Mean Fluorescence Intensities (MFI) are displayed (n=5; n=3 for LNCaP only). . (C) Alexa Fluor®647-conjugated infectious particles (Dunlop strain) gIb2 VLP binding to MDDC (n=5). (D) Dose dependent binding of genotypes Ia (circle), Ib2 (square) and IVb1 (triangle) VLP to MDDC (n=5). (E) Alexa Fluor®647-conjugated genotypes Ia, Ib2 and IVb1 VLP (10^4 VLP/cell) binding to MDDC with (empty circles) or w/o (closed circles) treatment with 0.2U/mL neuraminidase from *Clostridium perfringens*, specifically cleaving α(2,3/6/8)-linked sialic acid. Data are represented as MFI ± SEM. Statistically significant results were marked by one or several asterisks according to the level of significance: *=p<0.05, **=p<0.01, ****=p<0.0001; one-way ANOVA with Tukey's multiple comparison tests.

bioRxiv preprint doi: https://doi.org/10.1101/2020.09.04.282426; this version posted September 4, 2020. The copyright holder for this preprint (which was not certified by peer review) is the author/funder, who has granted bioRxiv a license to display the preprint in perpetuity. It is made available under aCC-BY-NC-ND 4.0 International license.

795 **Figure 2:** High-resolution confocal images of genotype Ia BKPyV particles endocytosed in
796 MDDC. Three panels showing independent cells that contain intracellular dot-like or
797 amorphous tube-shaped (white asterisk) accumulations of Alexa Fluor®647-conjugated gIa
798 VLP (A) or BKPyV infectious particles (B; Dunlop strain). Images show focal planes extracted
799 from six different cells stacks (10^4 VLP/cell or 1FFU/cell respectively for VLP and infectious
800 particles; magenta). (C) Two distinct focal planes extracted from the cell stack from which the
801 image in the center of Figure 2A is shown. "1" and "2" indicate the tube-shaped structures
802 marked by asterisks in Figure 2A. (D) Amira 3D reconstruction of the cell represented in Figure
803 2A (center) showing round-shaped and pleiomorphous tube-shaped intracellular structures
804 containing Alexa Fluor®647-conjugated gIa VLP. Cell membranes were stained with
805 fluorescence-labelled WGA (Alexa Fluor®488 displayed in light blue) and nuclei were
806 counterstained with DAPI. High-resolution confocal images were obtained from the A1 Nikon
807 microscope equipped with a SIM module.
808
809 **Figure 3:** TEM reveals unlabeled BKPyV endocytosis into large round- and tube-shaped
810 vesicles in MDDC. (A) Micrograph showing a general view of a representative MDDC
811 incubated for 30 minutes at 37°C with 10^4 VLP/cell (gIb2). Noticeably, the cell contains
812 abundant tube-shaped structures. (B, C, D, E and G) Pleiomorphous or large round vesicles
813 containing VLP are shown at a higher magnification (G: x100,000-120,000). (F) This image
814 represents infectious BKPyV particles into macropinosome-like (round-shaped) and tube-
815 shaped vesicles (1FFU/cell). (D) and (E) Micrographs showing VLP internalization from the
816 cell surface into tube-shaped endosomes. Thin and bold arrows indicate particles and tube
817 formation respectively; asterisk indicate large vesicles resembling macropinosomes.
818 N=nucleus; mt=mitochondria. Scale bars are indicated for each micrograph.
819

bioRxiv preprint doi: https://doi.org/10.1101/2020.09.04.282426; this version posted September 4, 2020. The copyright holder for this preprint (which was not certified by peer review) is the author/funder, who has granted bioRxiv a license to display the preprint in perpetuity. It is made available under aCC-BY-NC-ND 4.0 International license.

820 **Figure 4:** BKPyV particles colocalize with EEA-1, GRAF-1 and CTxB in MDDC revealing an
821 unconventional endocytic pathway. (A) Confocal sections of MDDC incubated for 30 minutes
822 at 37°C with 10^4 fluorescent VLP/cell (magenta). EEA-1-positive endocytic vesicles were
823 stained after fixation (green). Nuclei were counterstained with DAPI (light blue). The
824 colocalization between VLP and EEA-1 is shown in white. (B) RGB profiles along two
825 measurement lines (1 and 2, showed in Figure 3A) analyzed with ImageJ software.
826 Colocalization is represented by merging blue and red (=magenta) representing VLP and green
827 histograms (1 pixel=88nm). (C) and (D) show respectively colocalization of BKPyV VLP with
828 GRAF-1 (bold white arrows) and Alexa Fluor®555-conjugated cholera toxin subunit B (CTxB;
829 2µg/mL; thin white arrows). Deconvoluted images are presented. Displayed data are
830 representative of three independent experiments.
831
832 **Figure 5:** MDDC do not support BKPyV infection but mediate its transmission to primary
833 hRPTEC. (A) Epifluorescence microscope images (x10 magnification) showing large T antigen
834 (LTAg) immunostaining (green) of hRPTEC and/or MDDC in various conditions indicated on
835 top of rows, respectively: hRPTEC alone (medium), MDDC alone (medium), BKPyV-infected
836 hRPTEC (MOI=0.1; approximately 200 particles/cell), non-infected hRPTEC layered with
837 BKPyV-infected MDDC (excess of virus, i.e. unbound virus, was removed by extensive washes
838 after a 2 hour-incubation of MDDC with virus) and BKPyV-infected MDDC (*idem* previous
839 condition). LTAg is revealed at seven days dpi. Brightfield images of the immunostaining are
840 shown in the first column. DC-SIGN (red) is a marker allowing to discriminate MDDC from
841 hRPTEC when necessary. Nuclei were counterstained with DAPI. (B) RT-qPCR data showing
842 the amplification of LTAg mRNA seven dpi in various conditions (similar to those presented
843 in Figure 6A; n=6). Of note, a condition with uninfected MDDC with uninfected hRPTEC has
844 been added here. (C) Western blot analysis of VP1 expression, as a late BKPyV infection event,

bioRxiv preprint doi: https://doi.org/10.1101/2020.09.04.282426; this version posted September 4, 2020. The copyright holder for this preprint (which was not certified by peer review) is the author/funder, who has granted bioRxiv a license to display the preprint in perpetuity. It is made available under aCC-BY-NC-ND 4.0 International license.

in cell lysates after three, five, and seven days post-infection. β actin was revealed similarly after membrane stripping as a loading control. Figures 5A and 5C are representative of three independent experiments.

Figure 6: BKPyV virions or BKPyV-infected cells fail to activate MDDC. (A) CD86 cell surface expression was assessed by flow cytometry on immature MDDC alone (circles) or cultured with VLP (squares; 10^3 particles/cell), BKPyV particles (triangles; 10^3 particles/cell) MVA (inverted triangles) or a TLR agonist cocktail (diamonds; 100ng/mL LPS and 1µg/mL R848 after 24 hours (n=6). (B) ELISA titration of IL-10, IL-12p70 and IL-8 in the supernatants of untreated or MDDC cultivated with VLP, BKPyV particles or R848/LPS (doses were similar to those employed in Figure 4a). (C) Cell surface expression of CD80, CD83, CD40, CCR6, CCR7 and the HLA-DR on MDDC alone (empty bars) or cultured for 24 hours with VLP (grey bars; 10^3 particles/cell) or LPS/R848 (black bars). Data are represented as MFI ± SEM. For each MFI, background, i.e. autofluorescence, is subtracted to calculate ΔMFI values displayed in this figure (n=4). (D) Similar to experiments in A. Apop=apoptotic cells. Apoptosis was induced by UVB-irradiation and apoptotic cell fragments were collected by centrifugation and extensive washing in PBS. (E) RNAseq analysis of differentially expressed genes between infected (one dpi) and non-infected MDDC. The dashed line represents a “ten counts per gene” limit above which gene expression is considered as robust. The Y axis represents the Log2 fold change in gene expression. Statistically significant results were marked by one or several asterisks according to the level of significance: ns=non-significant, *=$p<0.05$, **=$p<0.01$, ***=$p<0.001$, ****=$p<0.0001$; one-way ANOVA with Tukey’s multiple comparison tests.

Figure 7: Endocytosed BKPyV particles into MDDC are protected from serum neutralization. HCS automated counting to evaluate percentages of BKPyV-infected hRPTEC (=$LTAg^+$ cells)

bioRxiv preprint doi: https://doi.org/10.1101/2020.09.04.282426; this version posted September 4, 2020. The copyright holder for this preprint (which was not certified by peer review) is the author/funder, who has granted bioRxiv a license to display the preprint in perpetuity. It is made available under aCC-BY-NC-ND 4.0 International license.

in various conditions including *cis*- and *trans*-infection experiments but with or w/o sera from a non-controller patient (=control serum) or a controller patient (=neutralizing serum). Neutralizing antibody titers in this serum had been previously determined: between 1/200.000, 1/500.000 and 1/20.000 for genotypes Ia, Ib2 and IVc2 respectively (see the Materials and Methods section). Here, both sera were x1000-diluted. Sera were either added before or after incubation of the BKPyV suspension (Dunlop strain at MOI=0.1) with MDDC. Results represent mean values of the percentage of $LTAg^+$ hRPTEC ± SEM. Statistically significant results are marked by an asterisk; *=$p<0.05$; one-way ANOVA with Tukey's multiple comparison tests.

Figure 8: Blood and kidney $CD1c^+$ myeloid DC bind and transmit BKPyV to primary hRPTEC without getting infected. (A) Quantitative measurement of VLP positive cDC and plasmacytoid (pDC) DC in whole blood of healthy volunteers according to the gating strategy shown in Supplemental Figure 1. (B) Quantitative analysis of VLP binding to cDC with (closed squares) or w/o (closed circles) Fc receptor blockade. Dose-dependent BKPyV VLP (C) or infectious particles (D) binding to purified $CD1c^+$ cDC from blood or kidney of healthy individuals; the "control" condition means no VLP (grey circles). Black closed and empty circles represent 10^3 and 10^4 particles/cell respectively. The immunomagnetic cell sorting strategy is shown in Supplemental Figure 1. (E) CD86 cell surface expression assessed by flow cytometry on freshly isolated blood $CD1c^+$ DC cultured for 24 hours in medium alone (squares) or with VLP (triangles; 10^3 particles per cells), BKPyV particles (inverted triangles; ibid) or with LPS/R848 (diamonds; 100ng/mL LPS and 1µg/mL R848); n=4 distinct blood donors. (F) Quantitative assessment of the ability of $CD1c^+$ mDC from blood (grey dots) or kidney (black dots), ie from healthy blood donors and macroscopically healthy parts of resected human tumor-bearing kidneys, to capture and transfer BKPyV to hRPTEC as shown in Figure 6A. The percentage of

bioRxiv preprint doi: https://doi.org/10.1101/2020.09.04.282426; this version posted September 4, 2020. The copyright holder for this preprint (which was not certified by peer review) is the author/funder, who has granted bioRxiv a license to display the preprint in perpetuity. It is made available under aCC-BY-NC-ND 4.0 International license.

infected hRPTEC corresponds to the percentage of LTAg+ hRPTEC within total cells, ie DAPI counterstained nuclei (42), based on an automated counting on a HCS device. Data are represented as percentage of infection. Statistical analyses have been applied to comparisons between % of infected hRPTEC in coculture with cDC with or w/o cDC preincubation with the Dunlop strain. Statistically significant results are marked by an asterisk; *=$p<0.05$, **=$p<0.01$, ***=$p<0.001$; one-way ANOVA with Tukey's multiple comparison tests.

Supplemental material

Supplemental Figure 1: Gating strategy of myeloid (CD11c+ in CD45+, HLA-DR+, Lin- cells) and plasmacytoid DC (CD123+ in CD45+, HLA-DR+, Lin- cells) in whole blood of healthy volunteers. Cells were incubated with 2.5µg/mL of Alexa Fluor®647 coupled-VLP or the same volume of PBS (no VLP; 45 minutes at 4°C) and representative dot plots showing the percentage of VLP+ cells.

Supplemental Figure 2: Assessment of purity of freshly isolated CD1c+ DC from blood and kidney. (A) Gating and enrichment evaluation before and after immunomagnetic cell sorting of CD19- CD1c+ myeloid blood DC. (B) Similar dot plots showing the purity of CD1c+ myeloid DC from resected human kidneys before and after the FACS-assisted sorting. These results are representative of five different cell isolations from both blood and kidney compartments.

bioRxiv preprint doi: https://doi.org/10.1101/2020.09.04.282426; this version posted September 4, 2020. The copyright holder for this preprint (which was not certified by peer review) is the author/funder, who has granted bioRxiv a license to display the preprint in perpetuity. It is made available under aCC-BY-NC-ND 4.0 International license.

Figure 1:

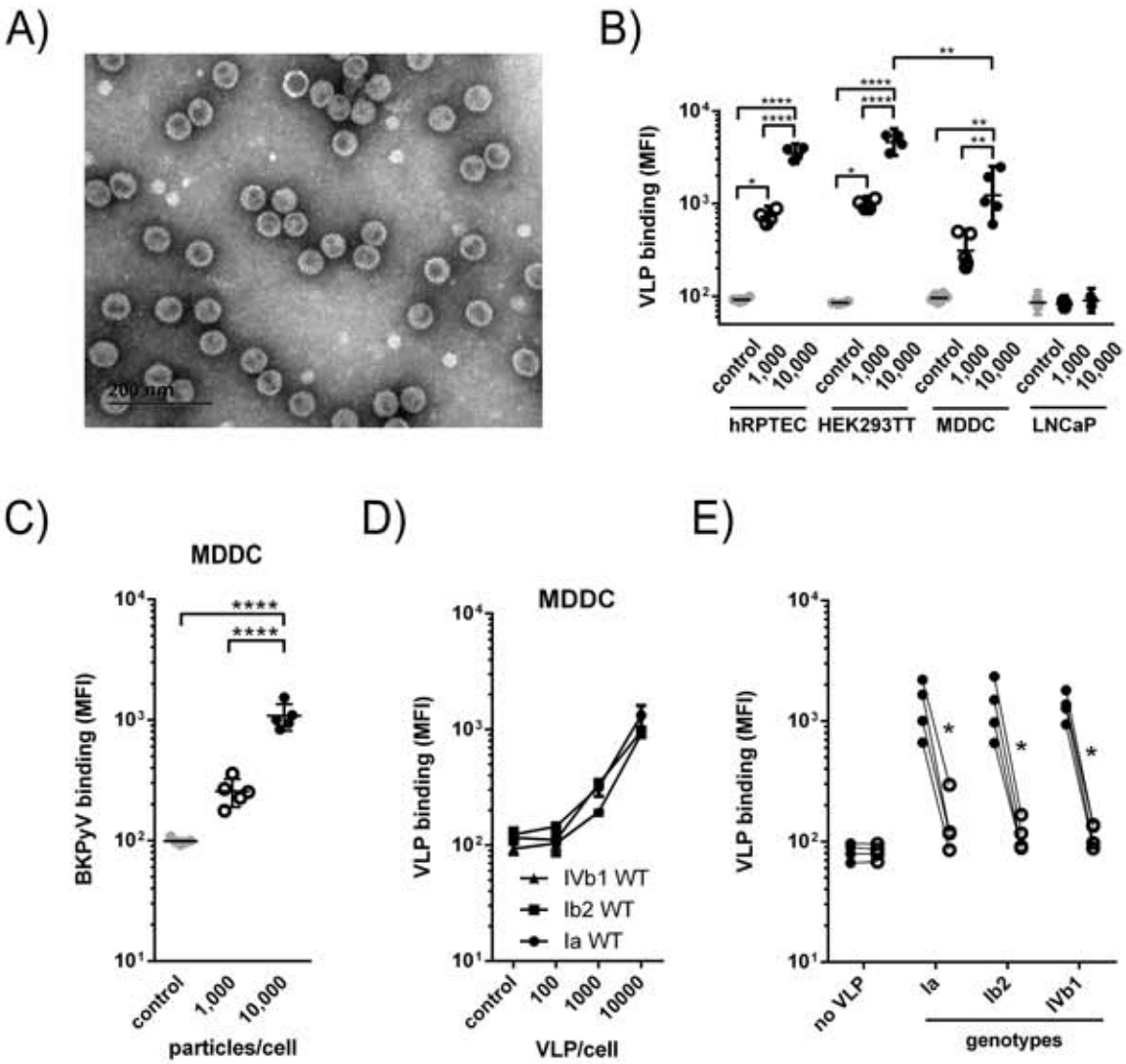

bioRxiv preprint doi: https://doi.org/10.1101/2020.09.04.282426; this version posted September 4, 2020. The copyright holder for this preprint (which was not certified by peer review) is the author/funder, who has granted bioRxiv a license to display the preprint in perpetuity. It is made available under aCC-BY-NC-ND 4.0 International license.

Figure 2

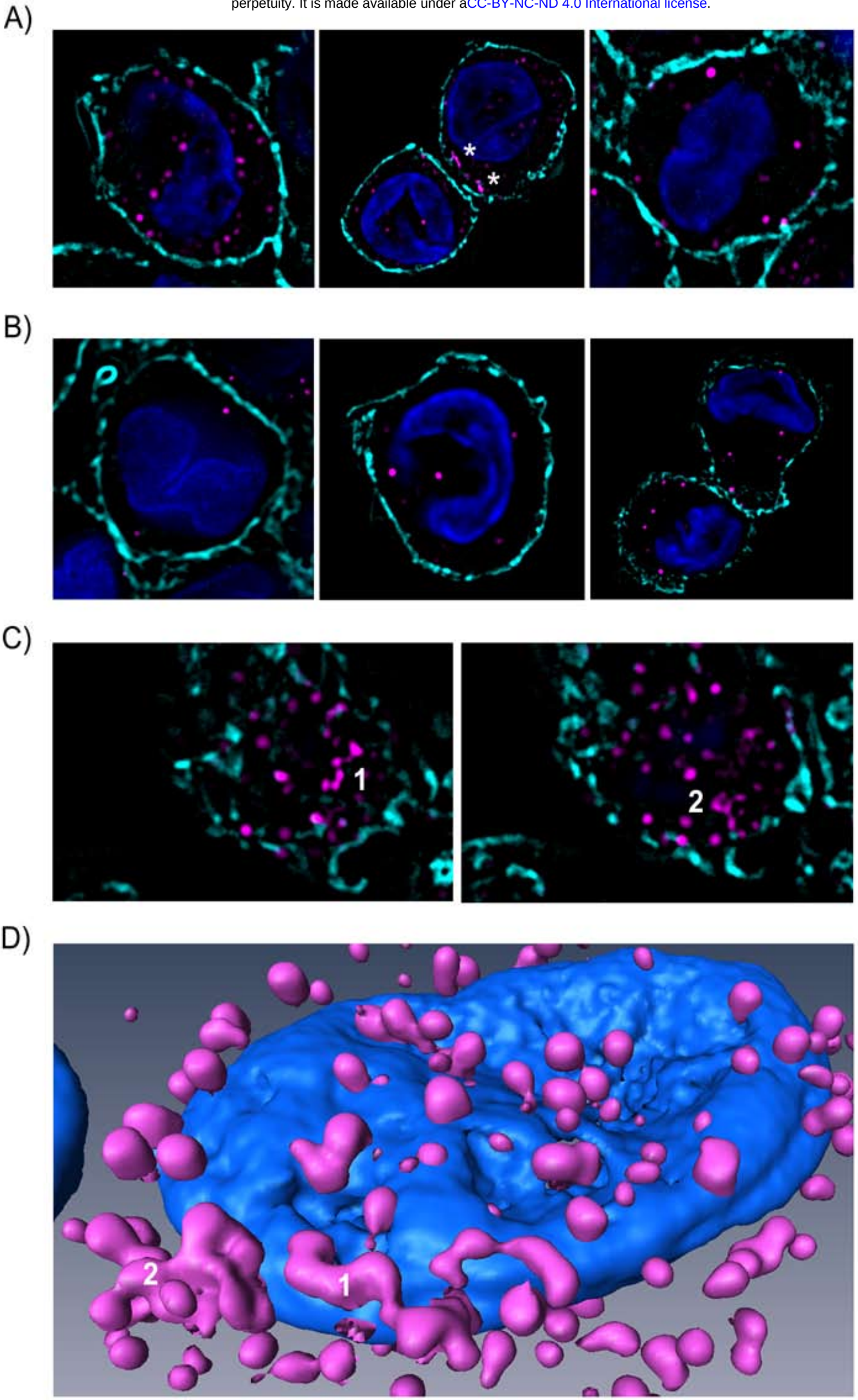

bioRxiv preprint doi: https://doi.org/10.1101/2020.09.04.282426; this version posted September 4, 2020. The copyright holder for this preprint (which was not certified by peer review) is the author/funder, who has granted bioRxiv a license to display the preprint in perpetuity. It is made available under aCC-BY-NC-ND 4.0 International license.

Figure 3:

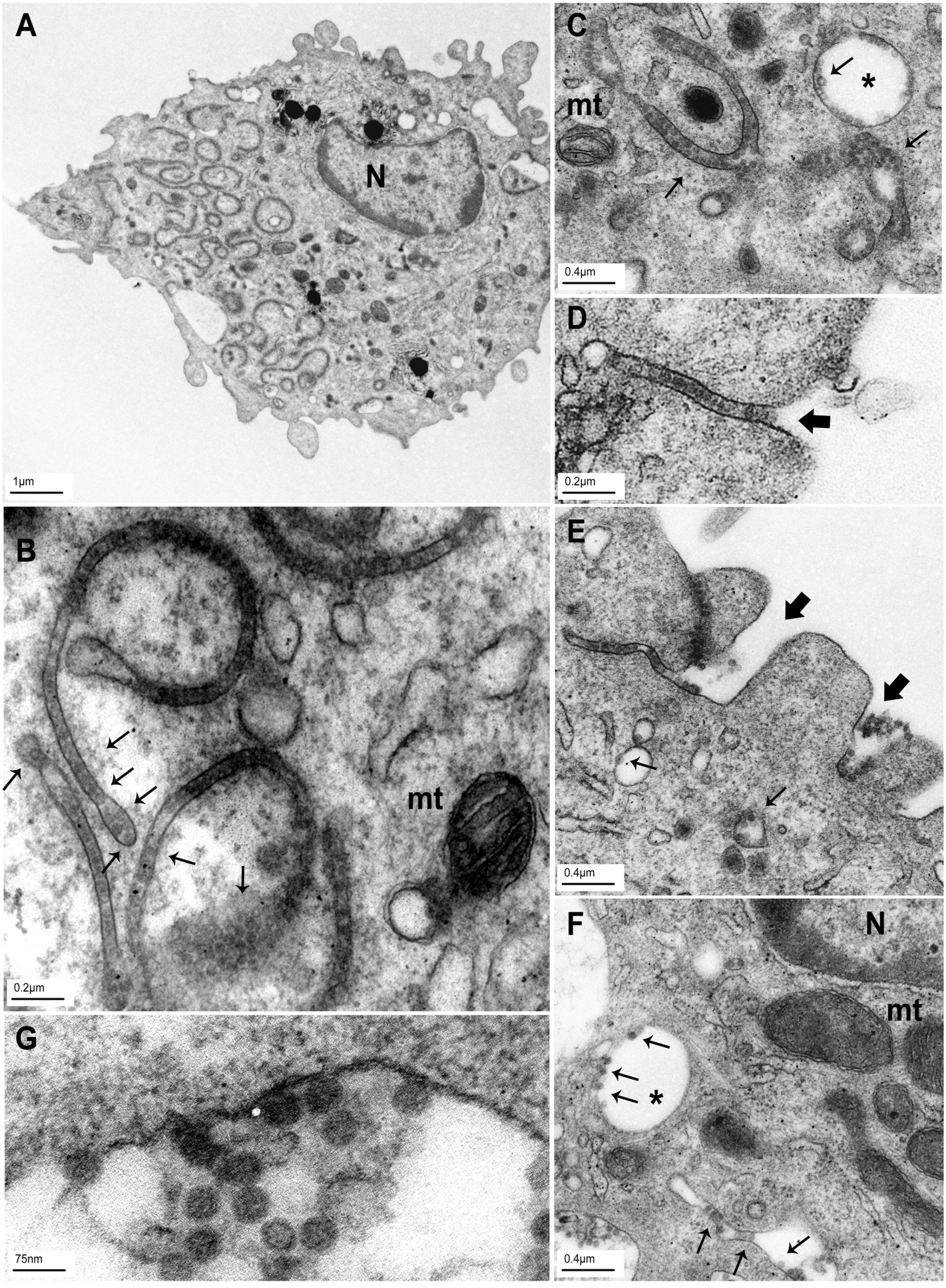

bioRxiv preprint doi: https://doi.org/10.1101/2020.09.04.282426; this version posted September 4, 2020. The copyright holder for this preprint (which was not certified by peer review) is the author/funder, who has granted bioRxiv a license to display the preprint in perpetuity. It is made available under aCC-BY-NC-ND 4.0 International license.

Figure 4

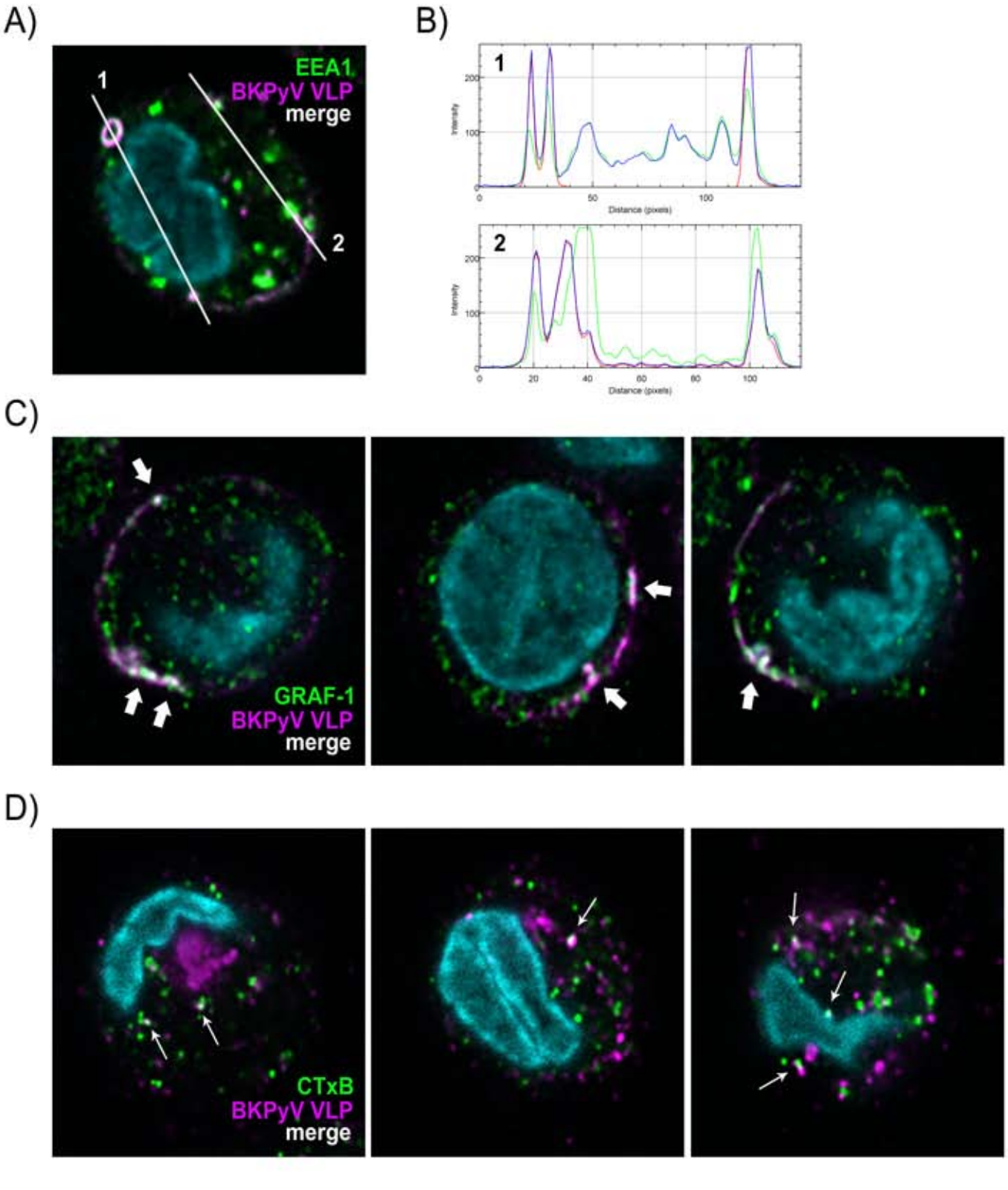

bioRxiv preprint doi: https://doi.org/10.1101/2020.09.04.282426; this version posted September 4, 2020. The copyright holder for this preprint (which was not certified by peer review) is the author/funder, who has granted bioRxiv a license to display the preprint in perpetuity. It is made available under aCC-BY-NC-ND 4.0 International license.

Figure 5:

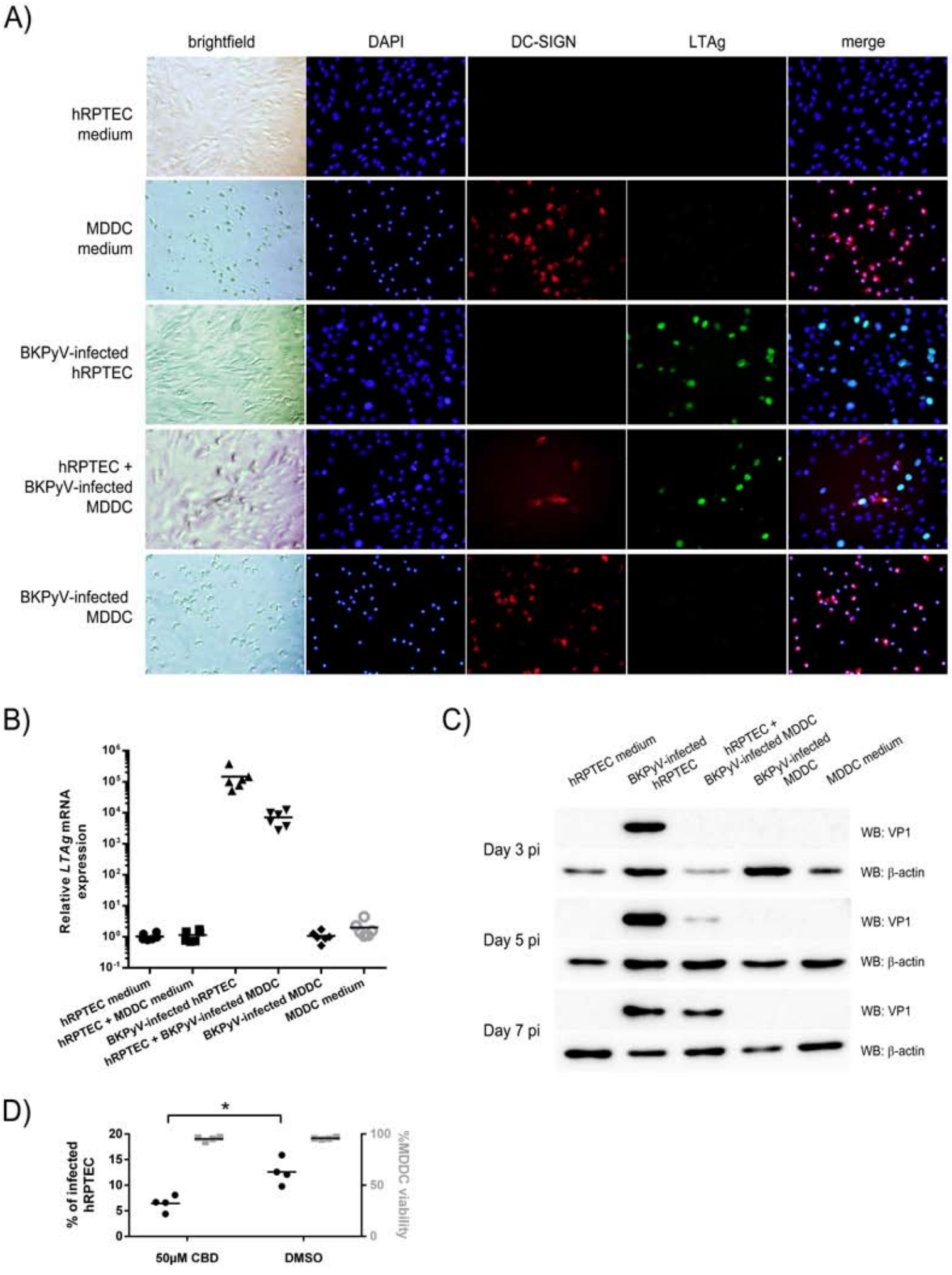

bioRxiv preprint doi: https://doi.org/10.1101/2020.09.04.282426; this version posted September 4, 2020. The copyright holder for this preprint (which was not certified by peer review) is the author/funder, who has granted bioRxiv a license to display the preprint in perpetuity. It is made available under aCC-BY-NC-ND 4.0 International license.

Figure 6:

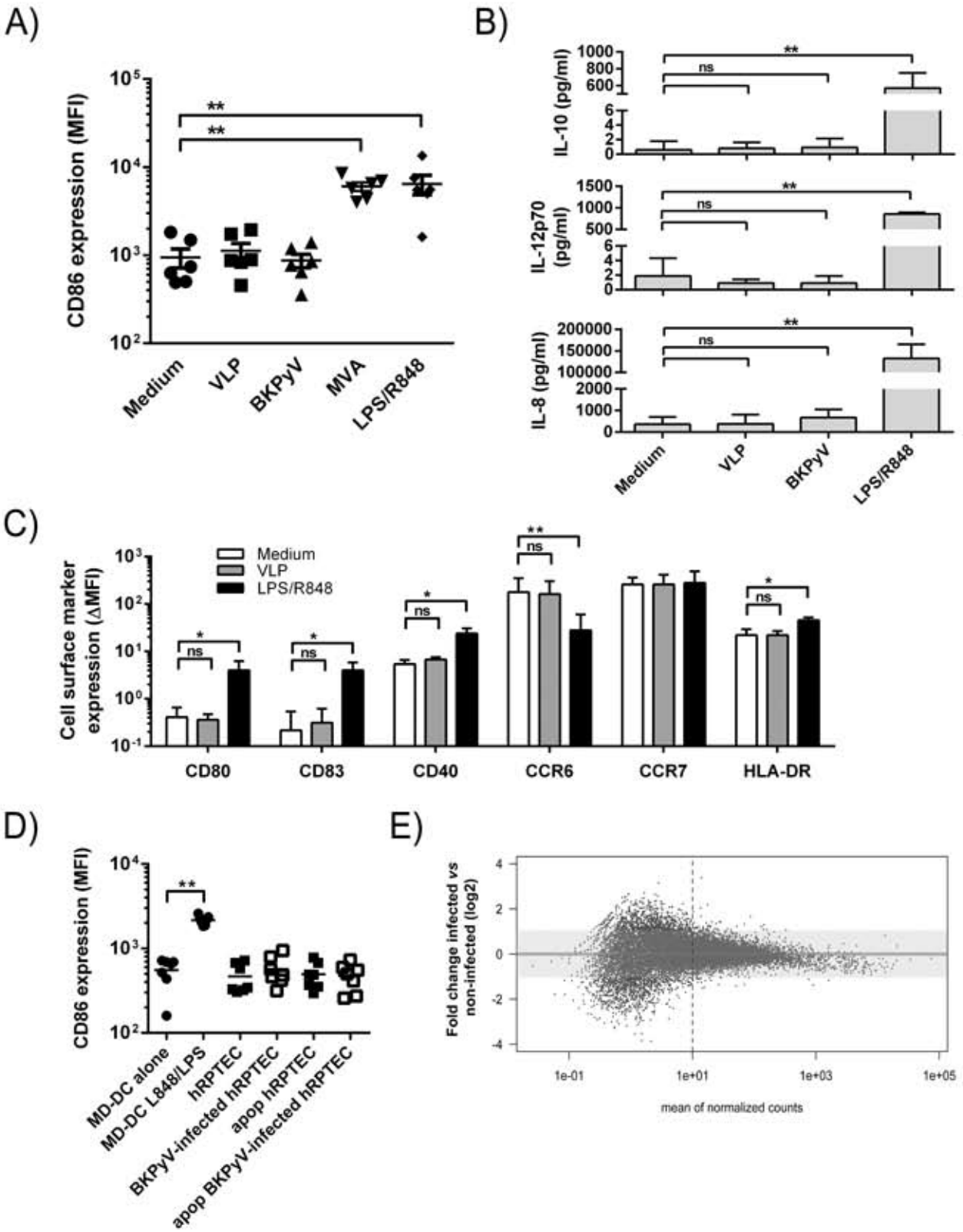

bioRxiv preprint doi: https://doi.org/10.1101/2020.09.04.282426; this version posted September 4, 2020. The copyright holder for this preprint (which was not certified by peer review) is the author/funder, who has granted bioRxiv a license to display the preprint in perpetuity. It is made available under aCC-BY-NC-ND 4.0 International license.

Figure 7

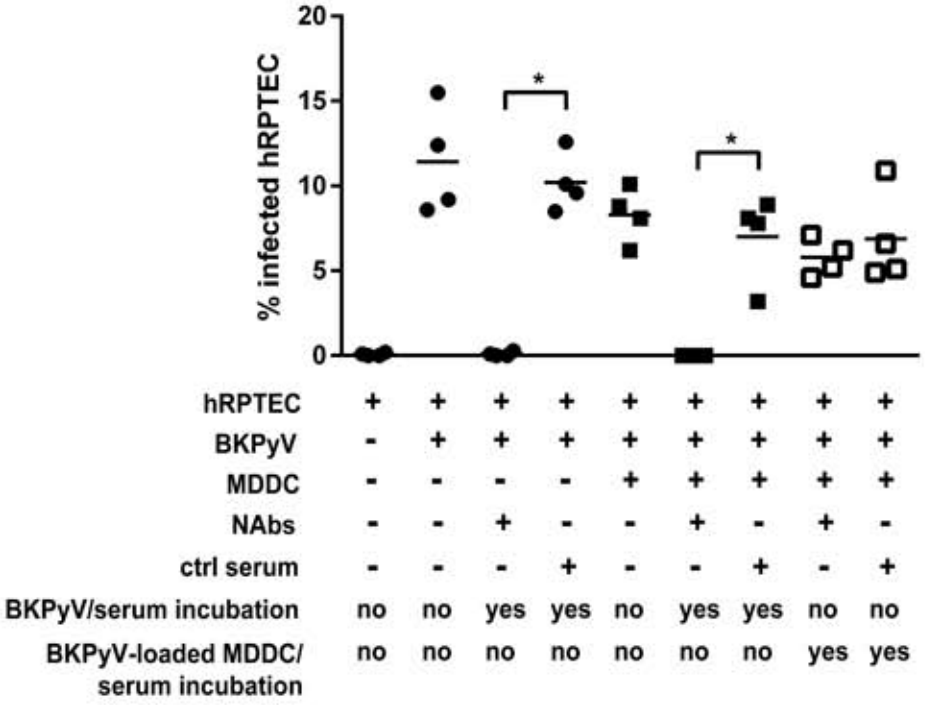

bioRxiv preprint doi: https://doi.org/10.1101/2020.09.04.282426; this version posted September 4, 2020. The copyright holder for this preprint (which was not certified by peer review) is the author/funder, who has granted bioRxiv a license to display the preprint in perpetuity. It is made available under aCC-BY-NC-ND 4.0 International license.

Figure 8: